SANDIA REPORT

SAND97-0674 • UC-706
Unlimited Release
Printed March 1997

High Accuracy Integrated Global Positioning System/Inertial Navigation System LDRD: Final Report

Todd E. Owen, Mark A. Meindl, J. Rick Fellerhoff

Prepared by
Sandia National Laboratories
Albuquerque, New Mexico 87185 and Livermore, California 94550

Sandia is a multiprogram laboratory operated by Sandia Corporation, a Lockheed Martin Company, for the United States Department of Energy under Contract DE-AC04-94AL85000.

Approved for public release; distribution is unlimited.

Sandia National Laboratories

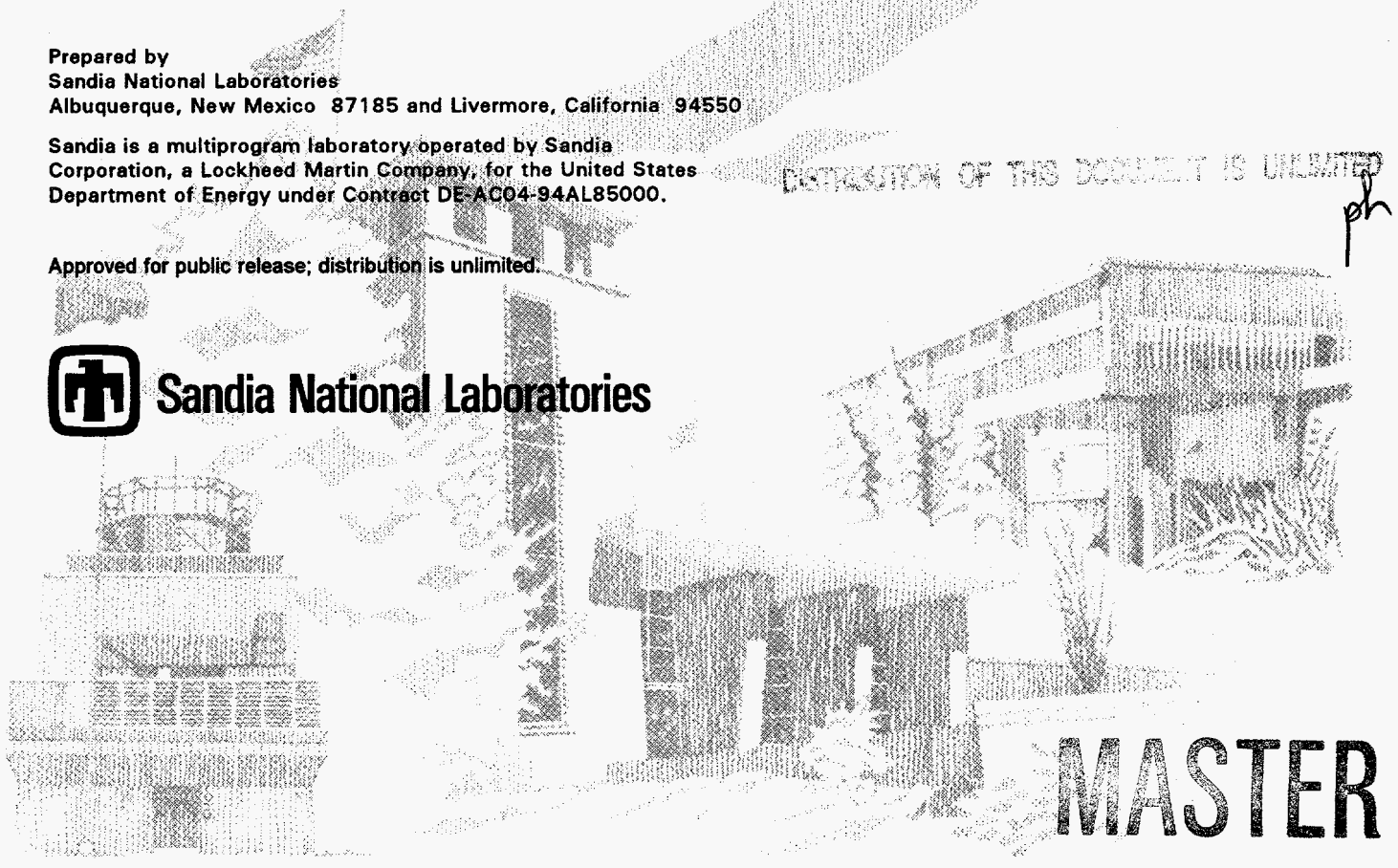

Issued by Sandia National Laboratories, operated for the United States Department of Energy by Sandia Corporation.

Available to DOE and DOE contractors from
Office of Scientific and Technical Information
P.O. Box 62
Oak Ridge, TN 37831

Prices available from (615) 576-8401, FTS 626-8401

Available to the public from
National Technical Information Service
U.S. Department of Commerce
5285 Port Royal Rd
Springfield, VA 22161

NTIS price codes
Printed copy: A03
Microfiche copy: A01

SAND97-0674
Unlimited Release
Printed March 1997

Distribution
Category UC-706

High Accuracy Integrated Global Positioning System/Inertial Navigation System LDRD: Final Report

Todd E. Owen
Mark A. Meindl
J. Rick Fellerhoff

Exploratory Systems Development Center
Sandia National Laboratories
P. O. Box 5800
Albuquerque, New Mexico 87185-0843

Abstract

This report contains the results of a Sandia National Laboratories Directed Research and Development (LDRD) program to investigate the integration of Global Positioning System (GPS) and inertial navigation system (INS) technologies toward the goal of optimizing the navigational accuracy of the combined GPS/INS system. The approach undertaken is to integrate the data from an INS, which has long term drifts, but excellent short term accuracy, with GPS carrier phase signal information, which is accurate to the sub-centimeter level, but requires continuous tracking of the GPS signals. The goal is to maintain a sub-meter accurate navigation solution while the vehicle is in motion by using the GPS measurements to estimate the INS' navigation errors and then using the refined INS data to aid the GPS carrier phase cycle slip detection and correction and bridge dropouts in the GPS data. The work was expanded to look at GPS-based attitude determination, using multiple GPS receivers and antennas on a single platform, as a possible navigation aid. Efforts included not only the development of data processing algorithms and software, but also the collection and analysis of GPS and INS flight data aboard a Twin Otter aircraft. Finally, the application of improved navigation system accuracy to synthetic aperture radar (SAR) target location is examined.

Acknowledgment

The authors would especially like to thank Dr. Elizabeth Cannon, Dr. Gerard Lachapelle, and Huangqi Sun from the University of Calgary, Canada, for their invaluable advice and analysis of the GPS carrier phase data. Also, we would like to thank Don Goodrich from Sandia for all of his hard work with the aircraft GPS antenna installations and flight safety support for the many flight tests necessary to collect the data for this research. We also thank the Sandians at the Tonopah Test Range for their help in supporting our flight testing there. Finally, a big thank you to the pilots, mechanics, and management of Ross Aviation, who operates the Twin Otter aircraft used for this testing, who were always ready to meet our flight test schedules and needs.

Contents

Figures

Tables

INTRODUCTION

1.1 High Accuracy Integrated GPS/INS System LDRD Description

The purpose of this Laboratory Directed Research and Development (LDRD) project was to explore the potential of real time, sub-meter level accuracy navigation by an integration of Global Positioning System (GPS) carrier phase signals with an inertial navigation system (INS). The low noise carrier phase GPS measurements are used to provide in-flight estimation of inertial navigation and component errors, and, in return, the calibrated INS can aid the tracking and can bridge short signal outage gaps in the GPS carrier signals. The work encompassed by this LDRD included not only the development of data processing algorithms and software, but also the collection and analysis of static and dynamic GPS and INS data collected aboard a twin engine aircraft. The recorded data was then analyzed, compared to an independent reference system, and post-processed to integrate the GPS and INS solutions.

Although the original intent of the LDRD was to then transfer to post-processing software over to a real-time system, that portion of the goal was not realized. The completion of the real time goal was affected by security restrictions in working with the data from a military, P-code GPS receiver. This was originally the primary receiver under investigation since it was already integrated, using only position and velocity navigation data, with a real time INS navigation system. It was hoped that the military receiver could supply the GPS carrier phase measurement accuracy in a stand alone mode when used with the cryptographic keys necessary to receive the more accurate P-code signals. It was discovered that, when the receiver is operated with the cryptographic keys, the GPS carrier phase data was classified and, as such, was difficult to work with. Therefore, the emphasis was switched to commercial, C/A code GPS receivers operating in a differential mode, with one receiver stationary at a surveyed site, and the second on the moving platform.

This change from an autonomous single GPS receiver to a pair of GPS receivers made the real time implementation more difficult and time consuming and, therefore, it was not completed for this project. However, the post processing software, written in 'C', to integrate the GPS carrier data from the pair of differential GPS receivers and the INS was developed and tested. The software has been shown to meet the accuracy and robustness goals necessary for a real-time airborne application and can be implemented in a real time flight computer in the future.

An additional area of research was added to investigate the potential of using multiple GPS receivers for attitude determination. Although the GPS carrier phase measurements from a single receiver directly provide accurate position and velocity measurements, any improvement in the overall GPS/INS system's attitude accuracy relies on estimating the INS' attitude errors from a Kalman filter. The Kalman filter compares the INS' and GPS' position and velocity measurements and then attempts to estimate the underlying INS attitude and instrument errors. If one could directly input GPS-derived attitude

measurements into the Kalman filter, there is the potential for either more accurately estimating the INS' attitude errors, or providing the opportunity for using a lower quality, less expensive INS whose inherent attitude error characteristics are poorer. To examine that potential, flight data was collected and analyzed to calculate GPS-based attitudes and compare those to the attitudes from a high quality INS to assess their potential for integration with and aiding of the INS.

1.2 Description of GPS Measurements

This section discusses the different types of measurements available from a GPS receiver: pseudorange, carrier phase, Doppler or phase rate, and the navigation (position and velocity) solution.

Pseudorange measurements are made by comparing a GPS receiver pseudorandom noise (PRN) code with the identical incoming code from a particular satellite to determine the time shift needed to correlate the two signals. This time shift can then be multiplied by the speed of light to determine the distance between the receiver and the satellite. This distance is called the pseudorange rather than true range since the GPS receiver and GPS satellite clocks are not synchronized and there is a range bias in the distance that is due to this clock difference.

The carrier phase measurement is made by differencing the satellite's PRN carrier frequency, either 1575 MHz for the L1 carrier or 1228 MHz for the L2 carrier, with the receiver generated carrier signal. The resulting beat phase is the difference in phase between the satellite and receiver at the time of measurement. Differencing of the carrier signals is much more accurate than the measurement of the pseudorange time difference, therefore the carrier phase has much lower noise characteristics. This phase difference, in carrier cycles or wavelengths, can be multiplied by the carrier wavelength, 19 cm for L1, 24.4 cm for L2, to obtain a distance measurement. Then, from one epoch to the next, the receiver integrates the number of carrier phase cycles measured and outputs the total integrated carrier phase cycles since the receiver began tracking the carrier signal.

There is a large uncertainty in relating this measurement to the true range between the satellite and the receiver, that is the number of complete cycles, N, between the receiver and a given satellite. This is called the carrier phase integer ambiguity. It is different for each satellite. The exact value of N for each satellite is not critical, but the difference in N for each receiver-satellite pair must be correctly estimated. Any common carrier phase integer number of cycles for all satellites may be removed as a clock bias term. Estimating the carrier phase integer ambiguity may be accomplished in a number of ways, the easiest being collecting a period, say 20 to 30 minutes, of data while the GPS receiver is stationary and then using a batch, least squares estimation technique to estimate the carrier phase integer ambiguity for each satellite. These ambiguities will then remain constant provided that no cycle slips occur over the observation period.

Cycle slips are the result of a loss of phase lock between the GPS receiver and the satellite and causes the carrier phase ambiguity to change by an integer number of cycles. Then, a new ambiguity number must be estimated, or the number of cycles slipped must

be measured. This drawback of carrier phase processing, the need for cycle slip detection and correction, is addressed in this research.

The Doppler frequency is a measure of the induced Doppler effect due the relative motion between the satellite and the receiver. It may be considered to be an instantaneous measure of the carrier phase rate.

The equations for the above measurement types are given below:

$$P = \rho + c(dt - dT) + d_{ion} + d_{trop} + d_p + \varepsilon P$$

$$\Phi = \rho + c(dt - dT) + N\lambda - d_{ion} + d_{trop} + d_p + \varepsilon \Phi$$

$$\dot{\Phi} = \dot{\rho} + c(\dot{dt} - \dot{dT}) - \dot{d}_{ion} + \dot{d}_{trop} + \dot{d}_p + \varepsilon\dot{\Phi}$$

where
P = pseudorange
Φ = carrier phase
ρ = the true satellite to receiver range
dt = the satellite clock error
dT = the receiver clock error
N = the carrier phase integer ambiguity
λ = the carrier phase wavelength
dion = the ionospheric error
dtrop = the troposheric error
dp = the satellite orbital error
ε = the measurement noise
$\dot{()}$ = denotes the time derivative.

A final output type from a GPS receiver, the computed time, position, and velocity, is not a direct measurement, but is the result of the receiver internally processing one or more of the above measurement types. For the receiver to autonomously compute its position or velocity, measurements from at least four satellites must be used. Three are needed to solve for the three position coordinates, and the fourth is needed to solve for the user's clock bias. GPS receivers typically use a Kalman filter to process the pseudorange and range rate measurements to arrive at an optimal estimation of their position, velocity, and time. The drawbacks to using the receiver's internally computed navigation solution are: (1) There must be measurements from at least four satellites or no complete navigation solution is obtainable, (2) The navigation solution may experience discontinuities with the inclusion or loss of satellite measurements, and (3) Because the outputs are those of a filtering process, assumptions about the magnitude and characteristics of the errors (i.e., uncorrelated, gaussian, etc.) are difficult to obtain and thus make their inclusion as measurements into another GPS/INS integration filter difficult to model.

2. FLIGHT TEST RESULTS

2.1 Tonopah Test Range Flight Tests

The first step in the research was to assess the GPS carrier phase measurements to verify that they were accurate enough to meet the 1 meter positioning goal. An independent system for accuracy determination was needed that was able to measure the position of the Sandia Twin Otter aircraft (see Figure 1), which was the airborne testbed for this research, to within one meter. The Sandia Tonopah Test Range (TTR), see Johnson (1996), has a high speed tracking camera, or theodolite, system with claimed accuracies that met that requirement. On June 9 and 10, 1993, GPS and theodolite data were recorded while the Twin Otter aircraft flew a series of figure eight patterns above TTR.

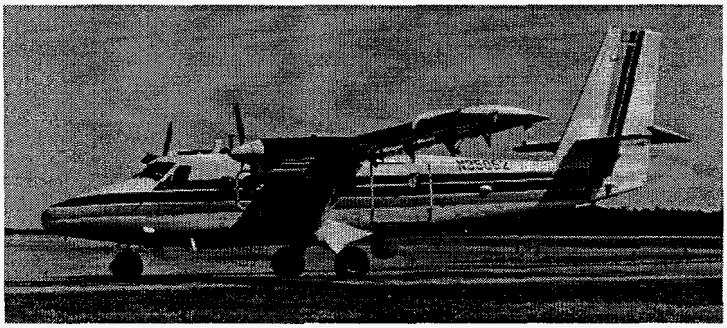

Figure 1. Sandia Twin Otter Aircraft

The system at TTR uses several theodolites, six for this test, at known locations, all of which communicate to a central computer system. As the aircraft flew, the theodolite operators simultaneously photographed the aircraft at a 5 hz rate. Each 35mm frame includes information regarding time and theodolite orientation. Theodolite time was synchronized to a central GPS timing receiver on the range. After a flight test, the 35mm film was developed and processed. The procedure required an operator to individually locate the aircraft nose on each frame of film and for every camera. This would require looking at 900 frames for 30 seconds of data. The data was then processed using triangulation to determine the position of the GPS antenna located on the fuselage of the aircraft. The accuracy of the TTR theodolite system depends on camera geometry and atmospheric conditions, but is quoted to be approximately 1 meter horizontally and 1.5 meters vertically. The flight tests to assess the GPS accuracy were flown soon after sunrise to minimize thermal effects.

The purpose of the data collection was to evaluate the accuracy of post processed differential carrier phase data from a commercial (C/A code) GPS receiver while flying aboard Sandia's Twin Otter aircraft. A NovAtel 10 Channel GPSCard receiver, model 951R, was flown aboard the aircraft and GPS range, range rate, and carrier phase data were recorded for post processing. A duplicate NovAtel GPS receiver was operated at a base station at TTR on a surveyed site.

Although several hours of data were collected over a two day period, due to the high cost and time involved with processing the theodolite data, only a 30 second linear segment and a 6.5 minute segment (one complete figure eight) of theodolite data were processed for data comparison purposes with the GPS systems. The NovAtel GPS data was post processed unsing C^{3}NAV™, a differential carrier smoothed pseudorange technique, and SEMIKIN™, a differential carrier phase processing software package, both developed at the University of Calgary. The expected accuracy of C^{3}NAV is in the 1 to 3 meter range and SEMIKIN in the sub-one meter range, but SEMIKIN is more susceptible to GPS carrier phase cycle slips and therefore less robust in a dynamic aircraft environment. The following table summarizes the results of the comparison with the theodolite derived positions:

Table 1. Comparison of Tonopah Theodolite Positions To Post-Processed NovAtel GPS Carrier Phase Derived Positions

GPS Carrier Phase Post Processing Method	30 Second Linear Segment Difference (meters)			Figure Eight Trajectory Difference (meters)		
	latitude mean/std	longitude mean/std	altitude mean/std	latitude mean/std	longitude mean/std	altitude mean/std
C^{3}NAV	0.28/0.08	0.01/0.09	3.10/0.06	-0.94/0.61	-0.60/0.59	3.41/0.53
SEMIKIN	0.55/0.18	0.22/0.09	3.49/0.04	-0.77/1.49	0.73/0.89	3.74/0.23

For both the C^{3}NAV™ and SEMIKIN™ differential post-processed NovAtel GPS data, the horizontal differences between their solutions and the theodolite data have mean values of less than one meter and one sigma standard deviations of less than one and a half meters. The larger differences occurred during turns in the figure 8 pattern and are likely due to small timing differences between the post processed GPS carrier phase data and the theodolite data. Comparison of the vertical position differences between the NovAtel data and the theodolite data show standard deviations ranging from one tenth to slightly over on half a meter, but indicate an approximate three and a half meter bias between the two solutions. It is thought that this bias is due to a difference in the method used to compute the height between the GPS solutions, which are based on height above ellipsoid, and the theodolite data which was based on a height above sea level coordinate system and which was transformed to the GPS-based coordinate system.

In summary, the Tonopah theodolite testing verified that, in an airborne environment, the positions derived from post processed GPS differential carrier phase data where near, or at, the one meter accuracy level when compared to an established, independent tracking system.

2.2 Integration of GPS and INS Data Flight Tests

The next step was to integrate the GPS carrier phase measurements with data from an INS which was also aboard the aircraft. The integration strategy used was to update the INS with GPS double difference carrier phase measurements in a centralized filtering approach, and to use the INS for GPS cycle slip detection and correction.

A flight test was conducted to investigate this methodology with the Sandia Twin Otter system.

2.2.1 GPS/INS System Description

The GPS/INS system consists of a Honeywell ring laser gyro (RLGA) inertial measurement unit (IMU), two NovAtel GPSCard™ GPS receivers and a Sandia Airborne Computer (SANDAC) as well as integration and guidance software systems. The RLGA is a product of a joint Honeywell/Sandia program to develop a small, lightweight, strapdown or roll stabilized, ring laser gyro IMU. It was operated in a strapdown mode for these tests.

The SANDAC consists of multiple processor modules, each using the Motorola MC68020 microprocessor and 68882 floating-point coprocessor, along with 128 kbytes of local memory. The GPSCard™ receivers are 10 channel C/A code systems which utilize a narrow-correlator spacing technology for improved code resolution and multipath rejection. It also outputs the raw carrier phase observable which was required for the current application. Timing between the GPS subsystem and the SANDAC computer clock was accomplished through a GPS 1 pulse-per-second interrupt, which gave a time tagging accuracy of several milliseconds between the GPS and INS data. For further information on the Sandia GPS/INS system, see Owen and Wardlaw (1992) and Fellerhoff and Kohler (1992).

2.2.2 Flight Test Description

A flight test was conducted at SNL/New Mexico in which the system described above was installed in Sandia's Twin Otter aircraft. About 2.5 hours of data were recorded during the mission over Kirtland Air Force Base. A 15 minute static survey was performed before and after the flight test in order to provide for GPS carrier phase ambiguity resolution. The aircraft reached an altitude of 350 m above ground and performed several maneuvers during the flight. Figure 2 shows the aircraft trajectory. A monitor GPS receiver was located 7 km from the runway and the separation between the monitor and aircraft ranged from 1 to 19 km.

Four to seven satellites were tracked above a ten degree cutoff elevation and the GDOP varied between 1.3 and 4.5. Outages in satellite availability generally occurred during turns when the antenna was shaded with respect to certain satellites, however at least four satellites were visible at all times. Raw GPS data was recorded at a 1 Hz rate, while INS position, velocity and attitude information was logged at 4 Hz.

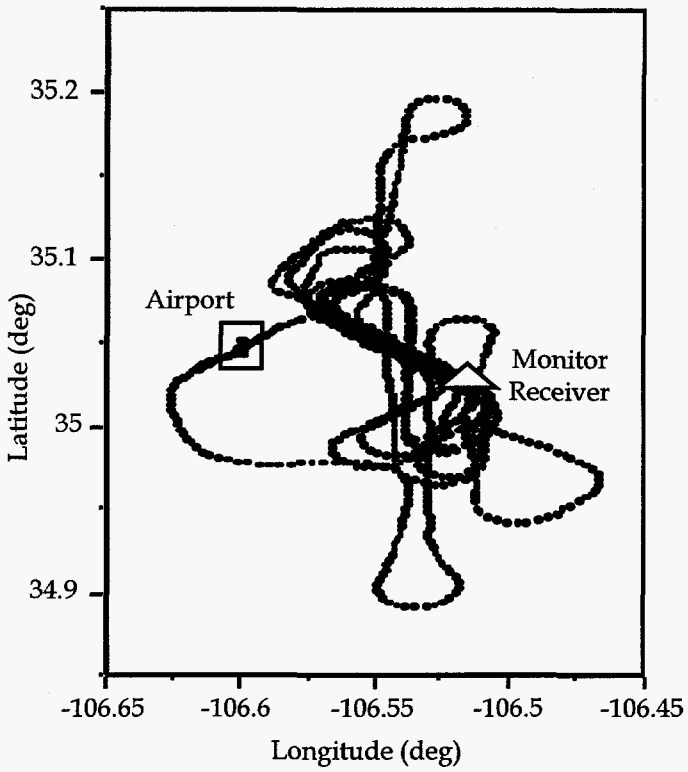

Figure 2. Aircraft Trajectory During GPS/INS Flight Test

2.2.3 GPS Only Results

The GPS data was first processed independent of the INS data in order to assess the accuracy of the stand-alone system. The University of Calgary's SEMIKIN™ program, which employs a double difference carrier phase model for static and kinematic positioning, was used in the data reduction (Cannon, 1990).

By double difference carrier phase measurements, we mean that, for a given GPS satellite, the phase measurements between two different receivers, in this case one on the ground and one in the aircraft, observing the same satellite are first differenced. This eliminates the GPS satellite clock error since it is common between the two measurements taken at the two different receivers. Then, a pair of these "between receiver single difference" measurements are differenced between two different satellites to yield a "double difference" measurement. The double difference eliminates the receiver clock error from the measurement since it is common between two satellites observed from a single receiver. The number of double difference measurements is equal to the number of common satellites tracked between the two receivers minus one and one satellite is usually chosen as the common, or base satellite, for the double differenced pair. For example, if GPS satellites # 6, 10, 12, 14, and 16 were being tracked at a given measurement epoch by both receivers, the double difference measurement combinations might be 6-10, 6-12, 6-14, and 6-16. Additional information on this technique can be found in Remondi (1984).

Carrier phase ambiguities (the integer number of carrier phase cycles or wavelengths representing the difference between the true range and the measured carrier phase) were resolved using the static initialization data prior to take-off. A least squares estimation processes is used, taking advantage of the changing geometry of the static receivers and the moving GPS satellites over the initialization period.

The occurrence of carrier phase cycle slips is a problem for accurate positioning of dynamic platforms. Carrier phase cycle slips occur due to antenna shading, vehicle acceleration, or other phenomenon and result in a loss of phase lock between the receiver and a satellite. When this occurs, the carrier phase ambiguity, which had been estimated at initialization, changes by an integer number of cycles and must be re-estimated.

For the GPS only case, the detection of cycle slips can be done with the phase rate method which compares the measured carrier phase with the predicted carrier phase. The predicted carrier phase is computed by the phase rate from the equation

$$\Phi_{k+1} = \Phi_k + \frac{\dot{\Phi}_k + \dot{\Phi}_{k+1}}{2} \Delta t ,$$

where Φ is the carrier phase measurement, $\dot{\Phi}$ is the phase rate measurement, and Δt is the time interval between k and k+1. The accuracy of this method is dependent on the dynamics of the aircraft since it assumes that the aircraft is constant during the time interval, which may not be a good approximation during takeoff, landing, or turns.

Following the detection of cycle slips, their correction in the GPS-only case can be done using satellites in which cycle slips do not occur as long as there are at least four cycle slip free satellites available. If so, these four satellites can be used to create a precise navigation solution and the carrier phase ambiguity can be directly estimated on the remaining satellite or satellites in which a cycle has occurred. However, if, at any time, fewer than four cycle slip free satellite measurements are available, the problem is more difficult and a dynamic estimation process must be used. This is where the integration of INS measurements is especially helpful, since the INS can provide information on the change in position from the last known "good" solution (i.e., before cycle slips) to the next time epoch containing good GPS data.

In the GPS data set analyzed for this flight test, at least four satellites were observed during the mission. Therefore, all cycle slips could be corrected, and a high level of positioning accuracy could be maintained.

The accuracy of the GPS results were assessed using three methods, namely (1) a check on the difference between the estimated GPS position at the end of the mission versus a batch GPS position computed from the stationary data at the end of the flight, (2) a comparison between forward and reverse time processing of the data, and (3) an analysis of the time series of the measurement residuals.

Using the first method, the ability of the processing algorithm to properly detect and correct cycle slips can be performed. If cycle slips are not corrected during a mission, a drift is induced into the estimated position results such that the final position at the end of

the run may be significantly offset from the true position. In the present case, the misclosure is at the several millimeter level, which suggests that all cycle slips have been correctly isolated.

The second technique where the data is processed in forward and reverse time is also informative. Since the aircraft trajectory should clearly be the same if processed in either direction, a comparison of the two trajectories provides quality assurance. Table 2 gives statistics between the forward and reverse time processing of the GPS data. The RMS is less than 1 cm in all three components which shows a high level of quality assurance in the GPS results.

Table 2. Statistics of Differences Between Forward and Reverse Time Processing of GPS Data

Component	Mean (mm)	RMS of (mm)
Latitude	0.2	1.1
Longitude	2.3	5.4
Height	-2.2	7.7

Figures 3 and 4 show residual time series plots for satellite pairs 24-16 and 24-20, respectively. Satellite 24 is the 'base' satellite which is common to all the double difference measurements. Figure 2 shows that all the residuals have an absolute magnitude less than 40 mm, which generally means that a high level of positional accuracy has been achieved. If cycle slips were not corrected in the data, discontinuities would be present in the residuals, and they would also drift significantly over time. Results for satellites 24-20 are similar to those in Figure 2. The mean and root mean square (RMS) for the misclosures in Figure 2 are -4 mm and 8 mm, respectively, while the values for Figure 3 are 1 mm and 10 mm, respectively.

The take-off and landing times are indicated on the figures to illustrate that the magnitude of the results are correlated to the distance from the monitor receiver as well as to the flying altitude. This is especially evident near the end of the mission where the aircraft increased altitude by a few hundred meters and the baseline separation was 19 km. Both figures show a large departure in the residuals at approximately 408000s when this occurs. As the aircraft descends and approaches the runway, the residuals resume a more typical level. Similar correlations to aircraft height and monitor separation can be found in Tiemeyer et al. (1994).

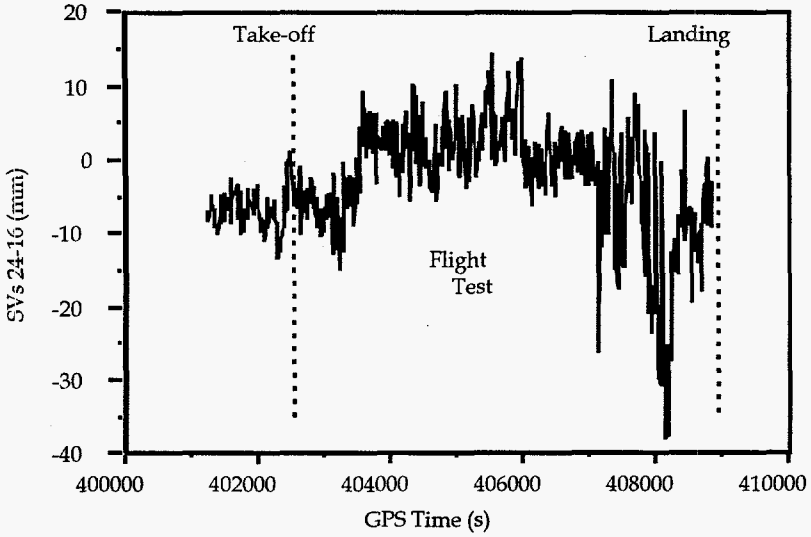

Figure 3. SVs 24-16 Carrier Phase Residuals

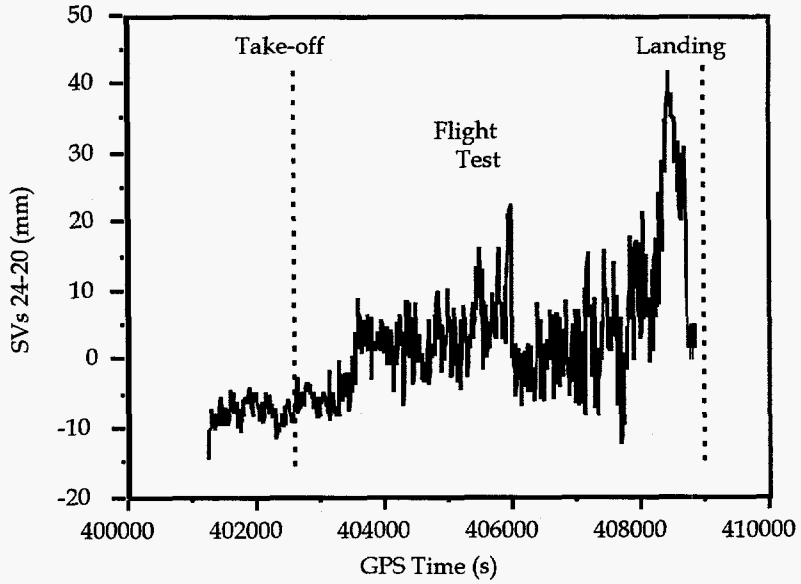

Figure 4: SVs 24-20 Carrier Phase Residuals

2.2.4 GPS/INS Integration Approach

The approach for GPS/INS integration follows the methodology similar to that described in Cannon (1991) where a 15 state Kalman filter was implemented containing three position error states, three velocity error states and three attitude error states as well as three accelerometer biases and three gyro drifts. One of the differences in the present implementation is that the available information from the INS consists of the integrated position, velocity and attitude estimates as compared to raw accelerometer and gyro output. An open loop design was used in which no information was used as feedback into the system. This design is not as optimal as a closed loop approach where the estimated IMU errors are removed from the IMU outputs, but it is more robust in the presence of erroneous GPS measurements in that the unaided navigation solution will never be corrupted by bad measurements that are not properly screened out.

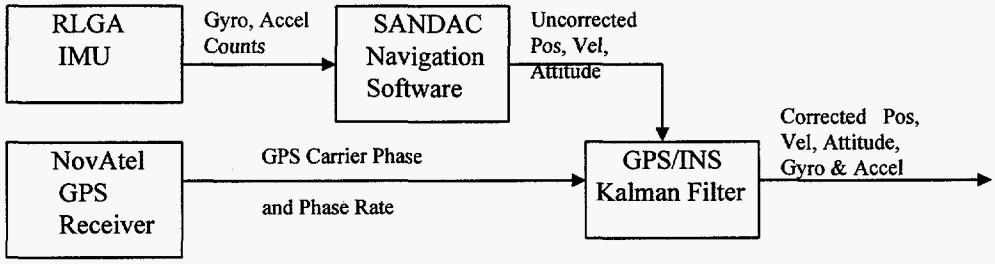

The integration of the GPS data into the filter was accomplished via a centralized approach whereby the double differenced GPS carrier phase and Doppler (phase rate) measurements are used as updates. No pseudoranges are used as measurement updates due to their noise level compared to the carrier phase data. In the current test data, the GPS double difference measurements were given an accuracy of 1.5 cm which accounted for residual tropospheric, ionospheric, orbital as well as multipath errors.

An inertial measurement unit can be described mathematically by modeling its error states. The IMU error vector, $\vec{x}$, can be written as

$$\vec{x} = \left[\delta\vec{p} \quad \delta\vec{v} \quad \delta\vec{a} \quad \delta\vec{b} \quad \delta\vec{i}_{imu}\right]^T$$

where

$\delta\vec{p} = \left[\delta \ln g \quad \delta lat \quad \delta h\right]$, (position errors)

$\delta\vec{v} = \left[\delta V_N \quad \delta V_E \quad \delta V_D\right]$, (velocity errors)

$\delta\vec{a} = \left[\delta_N \quad \delta_E \quad \delta_D\right]$, (attitude errors)

δb = barometric aiding state

$\delta\vec{i}_{imu}$ = IMU instrument errors

The first 9 elements of $\vec{x}$ are the differences between the true position, velocity, and attitude and the RLGA's position, velocity, and attitude. The barometric-aiding state

damps the instability of the altitude channel if an external aiding device is available. The remaining states depend on the quality of the RLGA instruments.

The IMU error dynamics are defined by the linear model

$$\dot{\vec{x}} = F\vec{x} + \vec{w}; \quad P = E\left[\vec{x}\vec{x}^T\right]; \quad Q = E\left[\vec{w}\vec{w}^t\right]$$

where $\vec{w}$ is a vector of independent, zero-mean, Gaussian-distributed random variables, P is the error covariance matrix, and Q is the process noise. the matrix F is the linearized error state dynamics matrix and is a time varying function of the trajectory.

The IMU covariance matrix is propagated by numerically integrating the continuous-time differential equation,

$$\dot{P} = FP + PF^T + Q.$$

The process noise used for the error states are listed in Table 3.

Table 3. Process Noise of Filter Error States

Parameters	Process Noise
Horizontal Velocities	0.0022 m/s/$\sqrt{s}$
Vertical Velocity	0.0032 m/s/$\sqrt{s}$
Misalignments	0.167 deg/$\sqrt{h}$
Gyro Drifts	1.2×10^{-4} deg/h/$\sqrt{h}$
Accel. Biases	3.7×10^{-5} m/s/$\sqrt{s}$

In general, the IMU errors will increase with time and the variances of these errors are governed by the previous equation. These errors can be reduced by using external measurements to update the IMU states. For this study, a Kalman filter was used to incorporate GPS carrier phase and rate measurements to reduce the IMU errors.

The linearized model for the measurements is

$$\vec{z} = H\vec{x} + \vec{v}; \quad R = E\left[\vec{v}\vec{v}^T\right]$$

where $\vec{z}$ is the measurement vector, $\vec{v}$ is a vector of independent, zero-mean, Gaussian noise, H is the measurement matrix, and R is the measurement noise matrix. The GPS updates define the structure of H.

For this work the measurement matrix, *H*, consists of the partial derivatives of the GPS observations, the double difference carrier phase and Doppler measurements, with respect

to the elements of the state vector, $\vec{x}$, for each satellite pair being tracked by both the base station receiver and the remote receiver, see Cannon (1991).

The Kalman gain equation and filter update equation are written as

$$K = PH^T\left(HPH^T + R\right)^{-1}$$

$$P^+ = (I - KH)P^-(I - KH)^T + KRK^t$$

where K is the Kalman gain matrix.

Finally, the error state vector, $\vec{x}$, may be updated as

$$\vec{x}^{\,+} = \vec{x}^{\,-} + \mathrm{K}(\vec{z} - \mathrm{H}\vec{x}^{\,-}).$$

2.2.5 GPS/INS Cycle Slip Determination Method

One of the main advantages of using an INS is the high relative accuracy which can be used to assist GPS cycle slip detection and correction. The INS can accurately predict the GPS antenna position at the measurement epoch which is then used in the computation of the 'approximate' double difference. This accurate approximation can thus be compared to the measured double difference to give a misclosure using the following relationship,

$$\delta = \frac{\Delta\nabla\rho}{\lambda} - \Delta\nabla\phi$$

where δ is the difference between the computed and measured double difference (cycles), $\Delta\nabla\rho$ is the computed double difference (m) calculated from the aided INS position solution, λ is the carrier phase wavelength (m/cycle), and $\Delta\nabla\phi$ is the measured GPS carrier phase double difference (cycles).

The absolute value of δ is then compared with a cutoff threshold to determine if cycle slips have occurred since the last GPS measurement epoch. Obviously, the threshold must be less than one cycle (approximately 20 cm) if positioning accuracies at the cm-level are required. If the threshold is larger, there is a risk that small cycle slips will not be detected in the GPS carrier phase data. Not only will positioning accuracies be reduced, the system reliability will be decreased since the statistics of the estimated quantities will not reflect the presence of undetected cycle slips. However, if the threshold is exceeded, the ambiguity on that particular double difference pair can be corrected by using the misclosure computed in the above equation.

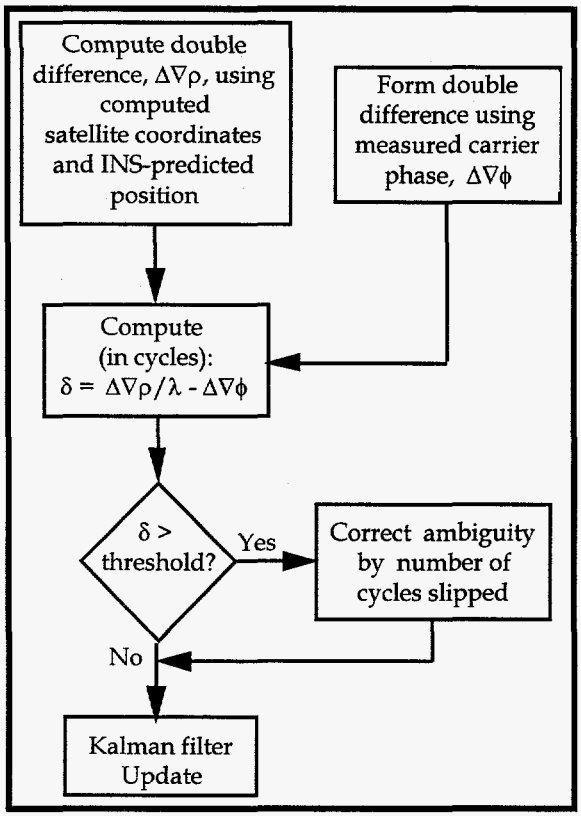

Figure 5. GPS/INS Cycle Slip Detection and Correction

In the GPS/INS case, it is not necessary to know on which satellite the slip occurred, i.e. the base or non-base satellite. The advantage of correcting the ambiguity instead of the raw data is that the correction is instantaneous, rather than correcting all subsequent measurements by the cycles slipped. Figure 5 summarizes the cycle slip detection and correction scheme. The benefit of GPS/INS integration for cycle slip detection and correction is that the number of satellites that have cycle slips at any one instant is not important. In contrast, GPS-only positioning requires at least four cycle-slip free measurements to detect cycle slips on the redundant measurements, or alternatively an effective on the fly ambiguity resolution process.

In order to correct cycle slips at the one cycle level, approximately 20 centimeters, the relative accuracy of the INS must be good to a few centimeters between GPS measurement epochs. Therefore, a high GPS data rate is beneficial to ensure that this accuracy criterion is met. Periods of satellite shading that cause GPS data gaps may reduce the ability of the INS to correct cycle slips below the one cycle threshold. Mis-synchronization between the GPS and INS sub-systems can also lead to difficulty in the cycle slip detection process.

2.2.6 GPS/INS Results

In order to show the effectiveness of the GPS/INS integration, differences between the GPS/INS position and GPS-only position are shown in Table 4. The position components agree to within a few centimeters while the velocity components compare to within 1.5 cm/s. These results indicate that the integration strategy is functioning correctly and that the GPS/INS system is providing a level of accuracy comparable to GPS when all cycle slips have been correctly resolved. The realized gain of integration is twofold, firstly to provide an accurate interpolator between GPS updates, and secondly to improve system reliability through accurate cycle slip detection and correction. This latter point is discussed in more detail below. Results achieved here are the level reported in Cannon (1991) using test data collected under similar conditions.

Table 4. Statistics of GPS-only Versus GPS/INS Results

Component	Mean of Difference	RMS of Difference
Latitude (cm)	1.3	1.3
Longitude (cm)	0.0	1.2
Height (cm)	-0.2	3.0
North Vel (cm/s)	-0.1	0.9
East Vel (cm/s)	-0.2	0.6
Vertical Vel (cm/s)	0.0	1.4

The INS error states, as estimated by the filter, showed east and north velocity errors to be less than 0.8 m/s, a heading error of approximately 0.125 degrees, and north and east tilt errors of approximately 0.05 degrees.

The cycle slip detection and correction capability of the INS can be measured through the misclosures between the GPS/INS predicted double differences and GPS measured double differences. Figure 6 gives these misclosures for the entire mission for two pairs of satellites, namely SVs 24-16 and 24-20, respectively. The first spike in the figures is due to the switch of a constant height constraint to a barometric height constraint which occurred at GPS time 401448 s. At 403610 s, effects of the switch from a barometric height constraint to single point GPS heights are evident.

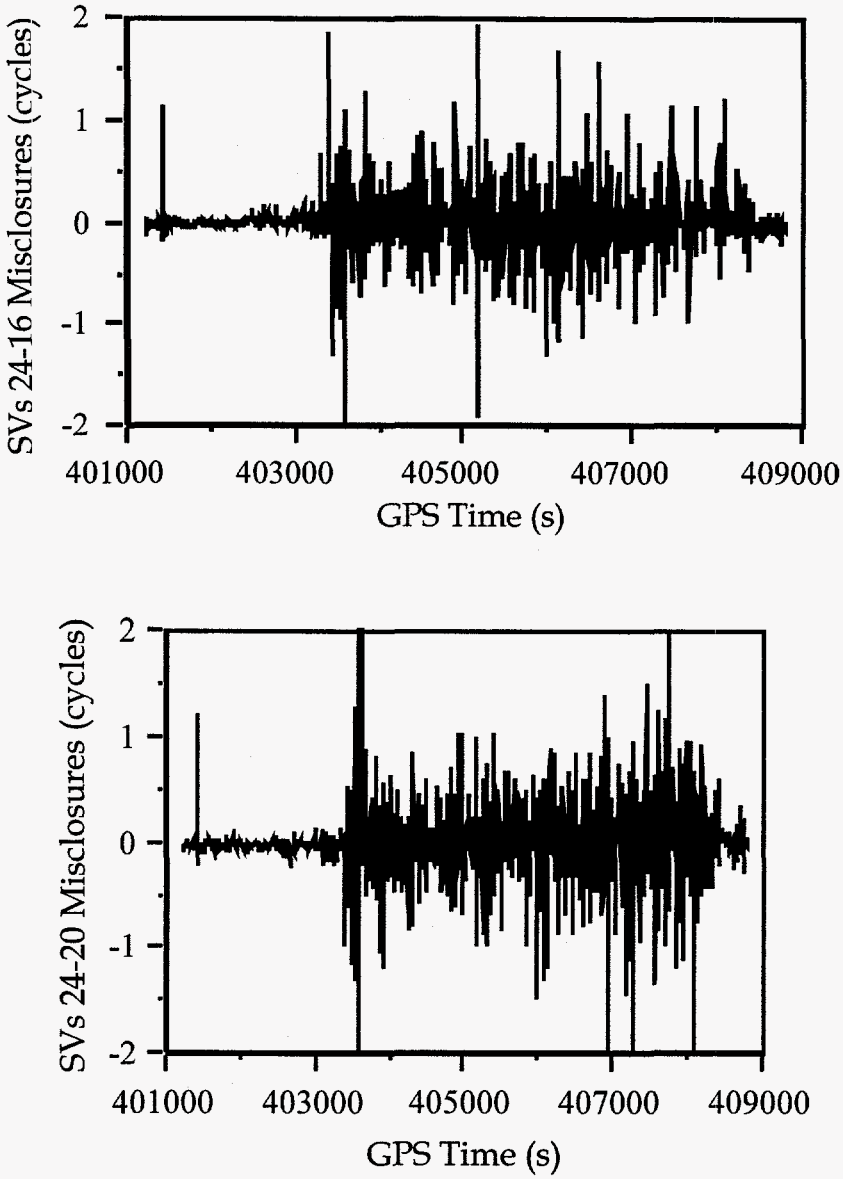

Figure 6. Misclosure Between Predicted and Measured Double Differences Using the Entire Flight Data

If only the static and taxi components are considered, the misclosures are smaller. Figure 7 illustrates these misclosures for SVs 24-20 before the aircraft takes off and shows that under static or low dynamic conditions, the accuracy of which the INS can precisely predict the GPS antenna position is very high and small cycle slips can be correctly determined.

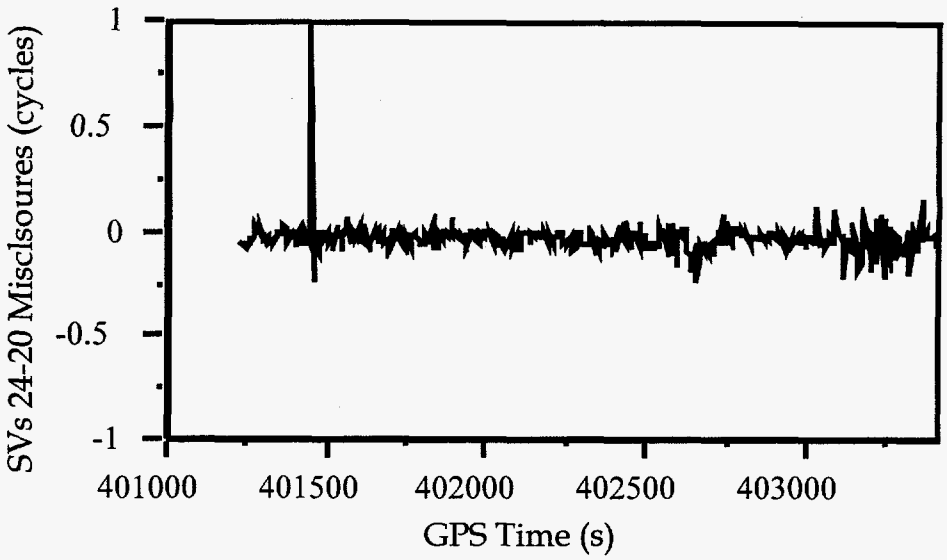

Figure 7. Misclosure Between Predicted and Measured Double Differences Using Static and Taxi Data for SVs 24-20

Table 5 summarizes the statistics of these misclosures for the entire data set, the static/taxi component as well as the in-flight data. It clearly shows that the misclosures are smaller on the static/taxi segments as compared to the in-flight data as evidenced in Figure 6.

Table 5. Misclosures Statistics for Satellites 24-16 and 24-20

Satellite Pair	Data Used	Mean of Misclosure (cycles)	RMS of Misclosure (cycles)
24-16	All	0.00	0.47
	Static/Taxi	0.00	0.27
	In-Flight	0.00	0.53
24-20	All	0.00	0.47
	Static/Taxi	-0.03	0.15
	In-Flight	0.01	0.54

The above results may be due to a residual time-tagging error between the GPS and INS subsystems. This is further investigated by analyzing flight data which includes straight and level data in addition to data collected during a turn. Figure 8 shows the misclosures for SVs 24-16 in these two cases. Misclosures are smaller for the straight and level data as compared to the data collected during turns which may be explained by a time tagging error at the 1-2 ms level. Results during the straight and level segment of data are comparable to those obtained in the static/taxi phase and show that accurate cycle slip

detection and correction with the GPS/INS is feasible in an airborne environment when time-tagging is precise.

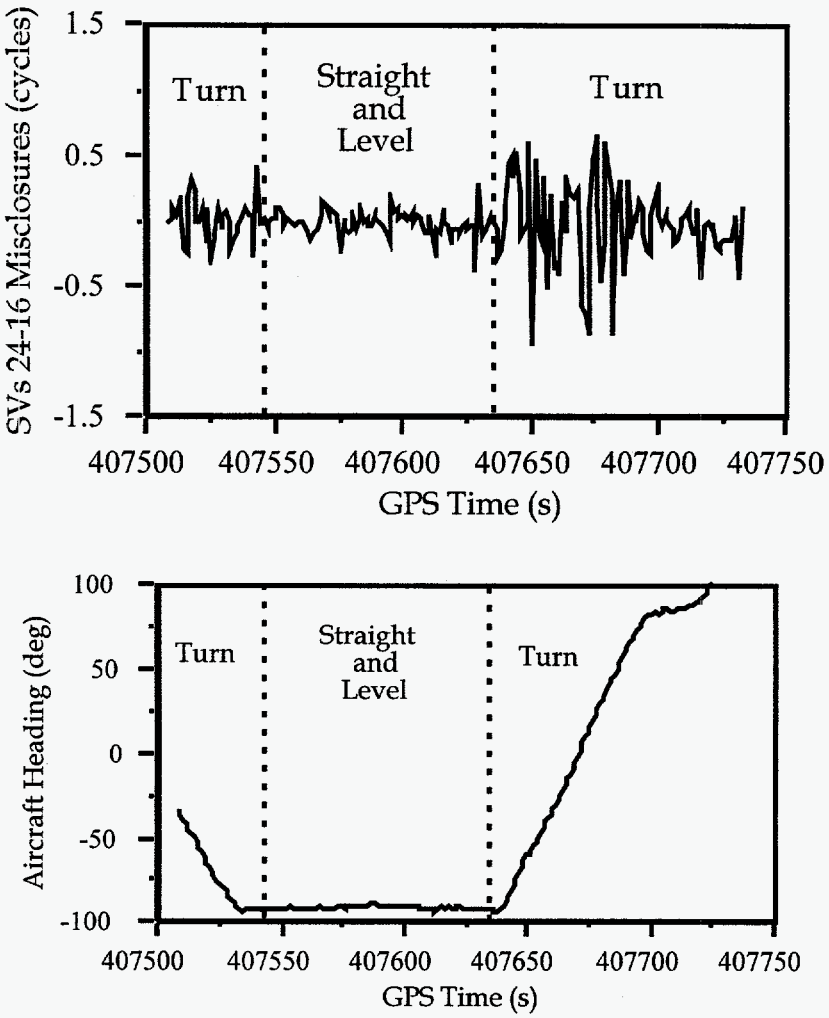

Figure 8. Difference Between Predicted and Measured Double Differences for SVs 24-16 and also Aircraft Heading Versus Time

2.2.7 GPS/INS Cycle Slip Detection and Correction Results

Several cycle slips were corrected in the GPS data in both the GPS-only processing as well through GPS/INS. Since four satellites were tracked throughout the mission, the GPS-only approach successfully handled these slips. Table 6 gives the number of cycles detected through GPS-only versus GPS/INS. When rounded to the nearest integer (since the slip has to be a multiple of a full cycle), both cases give the same result, which shows that the GPS/INS cycle slip detection and correction algorithm is working properly.

As previously discussed, one of the benefits of GPS/INS is that the number of satellites that simultaneously experience cycle slips is not relevant. In order to illustrate this concept, cycle slips of 1000 cycles were simulated in the aircraft carrier phase data for all satellites except for the base satellite at time 407544 s, during a straight and level segment of data. Table 7 shows the number of cycles detected by the GPS/INS system.

When the number of cycles is rounded to the nearest integer, the correct number of cycles are recovered in all cases, which means that the resulting trajectory is the same as the case when no cycle slips are present. It should be noted that algorithm will work as well for the case of only small cycle slips, i.e. it is not dependent on the number of cycles slipped. This demonstrates that multiple cycle slips are not a limiting factor in the achievable accuracy when an INS is used to complement a GPS-only approach.

Table 6. Cycles Detected by GPS and GPS/INS Systems

GPS Time (s)	SV	Cycles Detected GPS-only	Cycles Detected GPS/INS
403802	9	1590442.160	1590441.934
404479	9	9507533.099	9507533.394
404904	9	9524551.117	9524551.083
406197	12	1590511.123	1590510.903
406295	13	11173016.177	11173015.810
407508	3	5898676.981	5898677.049
407881	13	14495905.921	14495906.231

Table 7. Cycles Detected by GPS/INS System after Simulation of 1000 Cycles in Carrier Phase Data

Satellite Pair	Cycles Detected
24-16	1000.019
24-12	999.886
24-20	999.923
24-3	999.881

The data set with simulated cycle slips was then processed using only the GPS data. Since all satellites were affected, instantaneous ambiguity resolution was not possible and thus the ambiguities are estimated in the Kalman filter using the remainder of the data (Cannon, 1990). Differences between the GPS solution with no cycle slips versus the trajectory when the cycle slips are present are shown in Figure 9. A discontinuity is present when the slips occur and the error slowly decreases over time. This clearly shows that without the benefit of an INS, a GPS-only solution may be severely degraded. Current research into ambiguity resolution strategies may assist in the recovery of precise kinematic positioning after multiple cycle slips, however it is not currently possible to instantaneously resolve ambiguities, especially with single frequency receivers.

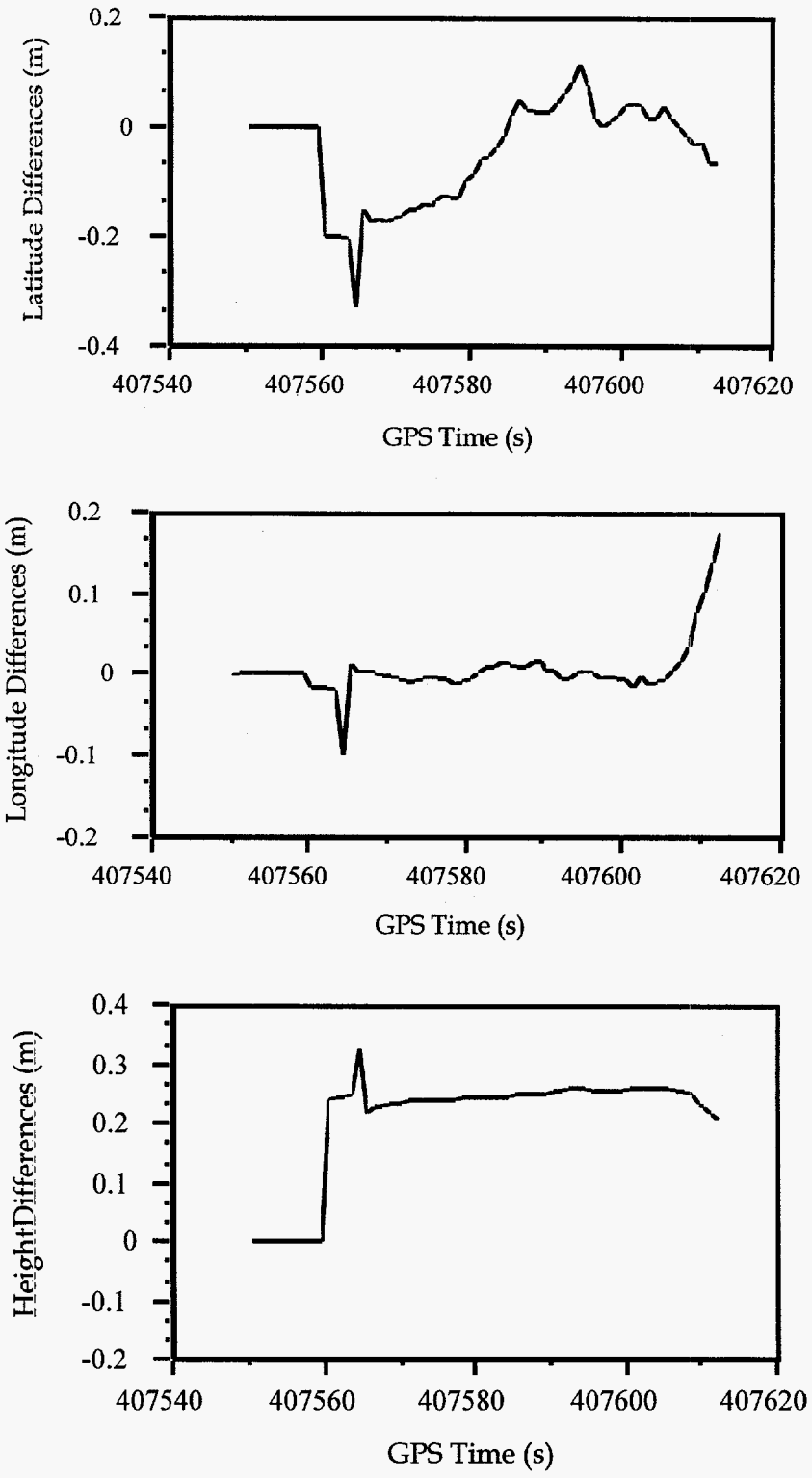

Figure 9. Error in Trajectory from GPS only Processing after Cycle Slip Simulation on all Satellites

2.2.8 Bridging GPS Outages

A final investigation into GPS/INS was performed to determine the effectiveness of the INS to bridge GPS outages. Although the INS has shown an accurate prediction capability when GPS updates are consistently available every 1 second, a typical scenario may be that the GPS signal is lost for several epochs. In this case, the INS error will be larger so that the ability to detect and thus correct GPS cycle slips at the 1 cycle level may be jeopardized. In order to test this, outages in the GPS data were simulated at time 407544 s for a period of 2 - 26 seconds. These data sets were then reprocessed and the misclosures between the predicted and computed double differences were calculated for each of the outage times. Figure 10 gives the misclosure as a function of the outage time for a two satellite pairs and shows that the longer the outage, the larger the misclosure, as expected. Effectively this figure illustrates the cycle slip correction capability which suggests that after about a 10 second outage, the INS prediction capability is not at the level needed to correct a cycle slip of 1 cycle. However, for many applications, a 10 second bridge may be sufficient. The noise in the figure is due to small time tagging errors in the data set, and in general the curves can be expected to be smoother. Also, with improved filter tuning, the outage time may be lengthened.

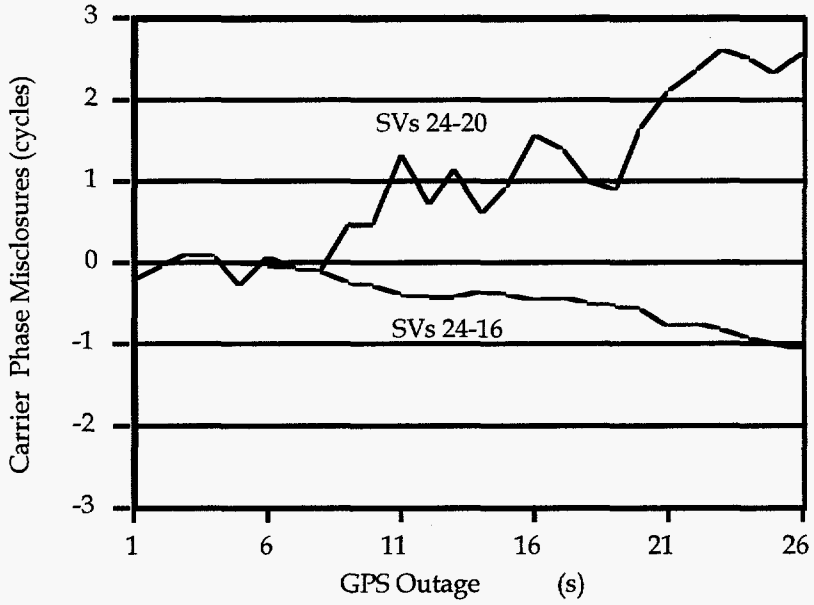

Figure 10. Phase Misclosure as a Function of GPS Outage

2.2.9 Conclusions of GPS/INS Integration Tests

Through the analysis of flight test data it has been shown that the GPS carrier phase data is of sufficient quality to provide high accuracy position results. Investigations into the trajectory misclosure, comparison of forward and reverse time processing, as well as measurement residuals were made to verify the quality of the results. Positions from GPS/INS positions agree at the cm-level with the GPS-only positions while the velocities agree below 1.5 cm/s.

The ability of the INS to accurately detect and correct GPS cycle slips was also demonstrated. Cycle slip correction by the GPS-only approach and the GPS/INS approach gave the same number of cycles which shows that the GPS/INS cycle slip methodology is functioning well. In addition, it has been demonstrated that in the case of multiple cycle slips when less than four satellites remain slip-free, the GPS-only accuracy is severely degraded, while the GPS/INS system correctly detected and corrected the slips so that a high level of accuracy was maintained. This illustrates the benefits of integration, namely improved accuracy and reliability.

2.2.10 GPS/INS Integration Software

The GPS/INS software which implements the algorithms described above has been written in C and is described in the following flowchart:

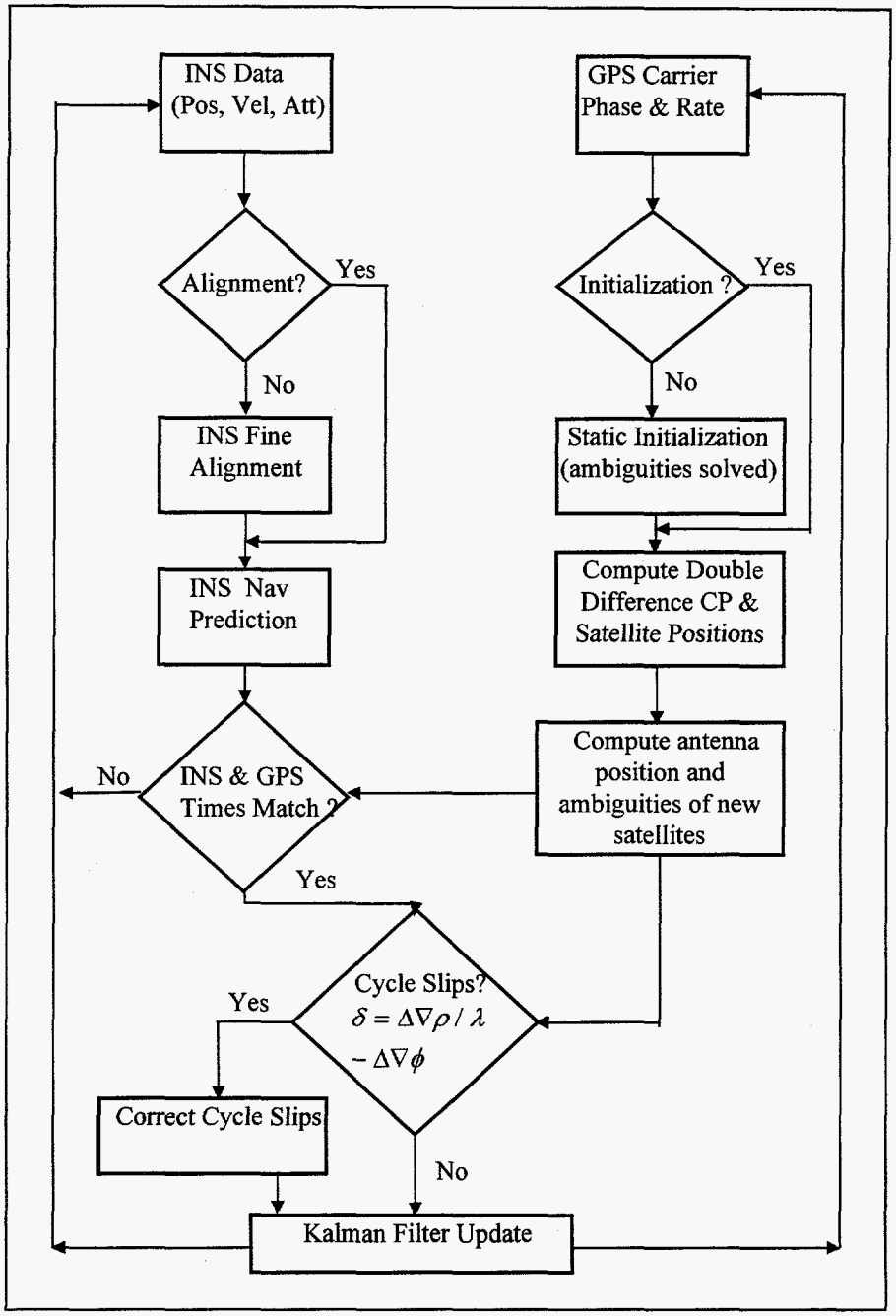

Figure 11. GPS/INS Software Flow Chart

The top blocks on each side of the software flow chart represent recorded INS position, velocity, and attitude data and recorded double difference GPS carrier phase data. If the INS has not already undergone a static alignment process in which zero velocity updates are used to initialize the estimate of attitude and accelerometer and gyro bias errors, that procedure is done. In parallel, while the aircraft is stationary, the initial GPS carrier phase ambiguities are determined as well. After these initialization procedures are complete, the INS solution is propagated forward in time and the GPS double difference carrier phase, satellite position, and velocity for the next measurement set are computed. This continues until the INS and GPS data time tags match (the INS data is usually

available at a higher rate than the GPS data). The INS position, velocity, and attitude are interpolated to match the GPS epoch and the estimated INS errors are propagated forward to this epoch time as well. Cycle slip detection and correction is performed using both the GPS double difference measurements and the predicted corrected INS solution. After correcting any GPS cycle slips, the double difference carrier phase is used to update the INS using the Kalman filter update equations. This process then continues until the end of the GPS or INS data.

Further GPS/INS development would include the transition of this post-processing methodology into a real-time system. This would entail both a communication link between the monitor and aircraft as well as optimization of the algorithms for improved efficiency.

2.3 GPS Attitude Determination Tests

The objective of this portion of the research was to assess the performance of a non-dedicated GPS attitude determination system in an operational aircraft environment. Comparisons are made between GPS attitude components and those obtained from an INS which was also installed in the aircraft. If the GPS-derived attitudes were on the same level of accuracy as those obtained by the more expensive INS, one could propose their integration into the GPS/INS Kalman filter in addition to the GPS carrier phase range and range rate measurements.

2.3.1 Test Description

For this series of tests, three single frequency GPS antennas were installed on the aircraft, one on each wing and one near the tail, in addition to the dual frequency GPS antenna already in place just aft of the cockpit. The locations of the four GPS antennas are shown in Figure 12.

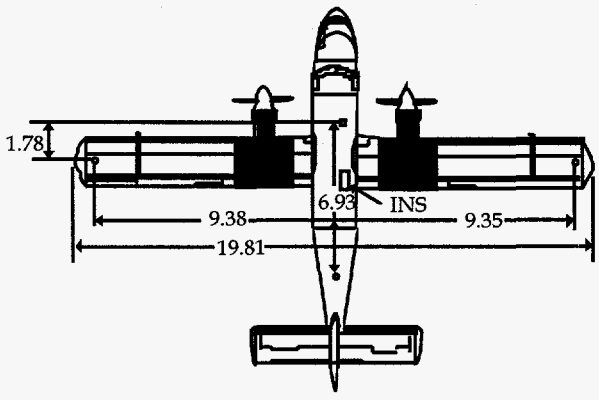

Figure 12. Aircraft Antenna Locations

The suite of test equipment included: 1) six NovAtel GPSCard™ receivers, each housed in a portable personal computer, four in the aircraft and two on the ground; 2) a Honeywell ring laser gyro assembly (RLGA) inertial measurement unit (IMU); 3) a Sandia Airborne Computer (SANDAC) to implement the navigation equations; and 4) a

Texas Instruments (TI) embedded P-code GPS receiver integrated with the SANDAC. The RLGA IMU and SANDAC were mounted on the floor of the aircraft just forward of the main cabin door.

Four portable computers containing the NovAtel GPSCards™ were mounted in the flight racks, with each receiver connected to one of the four GPS antennas. The TI embedded P-code receiver was connected to the dual frequency forward fuselage GPS antenna in parallel with one of the NovAtel receivers. The TI receiver's 1 pulse per second interrupt was used to time tag the SANDAC/RLGA navigation and attitude measurements to GPS time to an accuracy of a few milliseconds.

Two NovAtel ground station receivers were set up for kinematic testing purposes, e.g. Sun (1994). One antenna was mounted on an airport hangar while the second was set up at a surveyed benchmark approximately seven kilometers from the airport. These sites are indicated on Figure 13.

A static test was performed in order to compute the relative positions between the four aircraft antennas. Four flight tests were conducted as part of this experiment and two were selected for attitude post-processing. The test characteristics for these days, herein denoted as Day 3 and Day 4, are given below.

Day 3 Flight Test: Several high dynamic maneuvers were undertaken and midway into the flight, the airborne receivers were intentionally shut down and re-booted to assess the in-flight acquisition performance and to collect data to look at in-flight on-the-fly ambiguity resolution for kinematic positioning. GPS data was logged at 10 Hz and IMU data was logged at 10 2/3 Hz. The flight trajectory that was used in the analysis is shown in Figure 13 which includes the first part of the flight before the intentional shutdown. Roll, pitch and heading as estimated from GPS are shown in Figure 14. Pitch varied from 0 to 12 degrees while roll maneuvers were in the -30 to +20 degree range. The number of satellites tracked ranged from 4 to 7 during the segment of flight data that was analyzed.

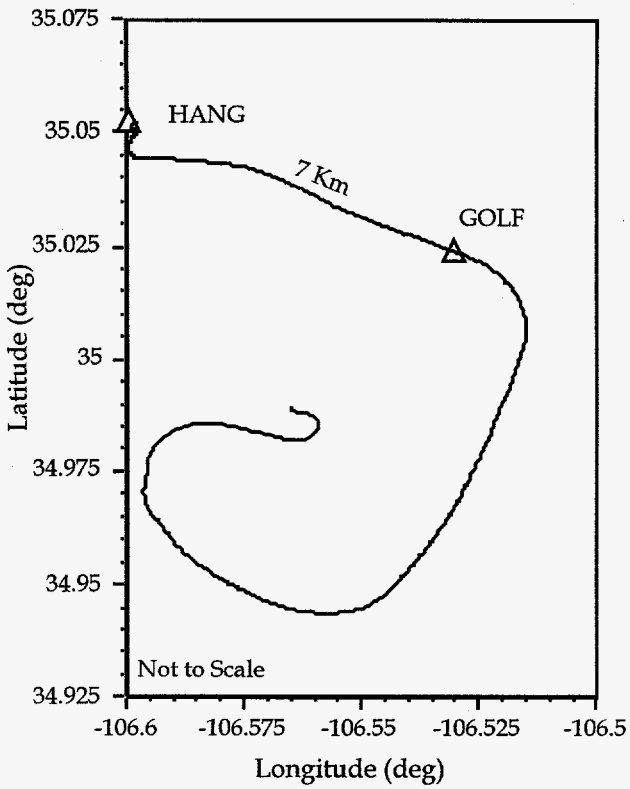

Figure 13. GPS-Based Attitude Testing: Aircraft Trajectory on Day 3

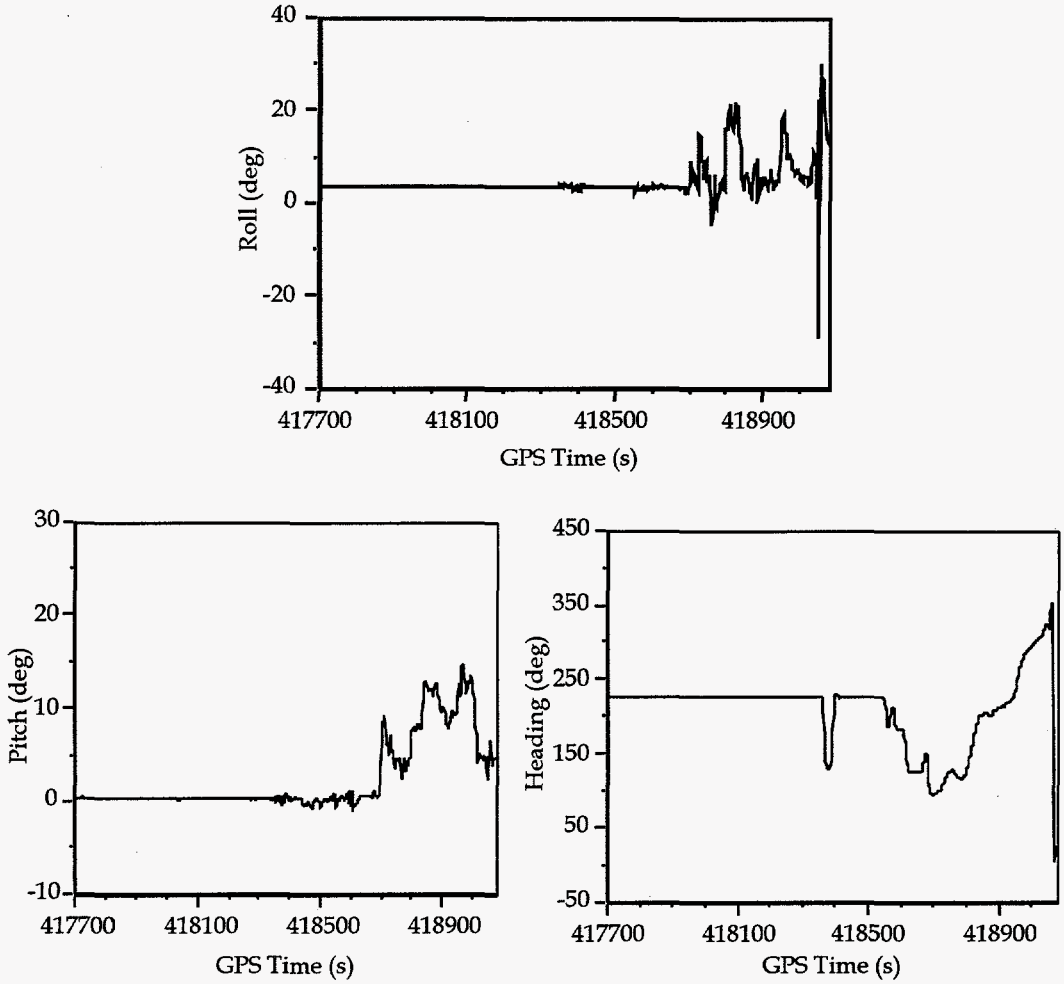

Figure 14. Aircraft Roll, Pitch and Heading on Day 3 Estimated from GPS

Day 4 Flight Test: For this test, the aircraft operated using low dynamic flight parameters. The flight's purpose was primarily to test the kinematic position performance over long baselines with multiple monitor stations and multiple aircraft receivers and antennas. GPS data was logged at 5 Hz and IMU data was logged at 8 Hz. The flight trajectory is shown in Figure 15 and the GPS attitude components are given in Figure 16. In this test, aircraft roll ranged from -40 to +45 degrees and pitch ranged from -5 to +12 degrees. Four to eight satellites were observed during the mission.

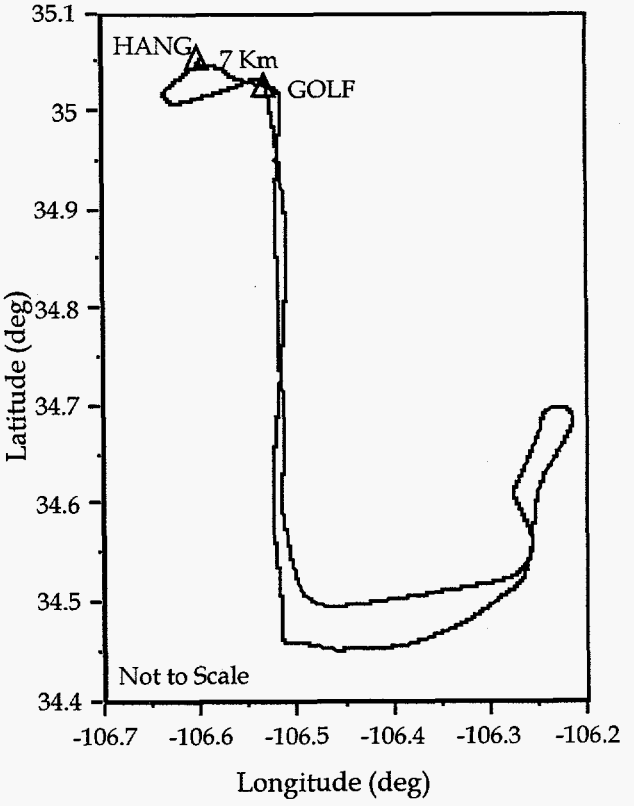

Figure 15. GPS-Based Attitude Testing: Aircraft Trajectory on Day 4

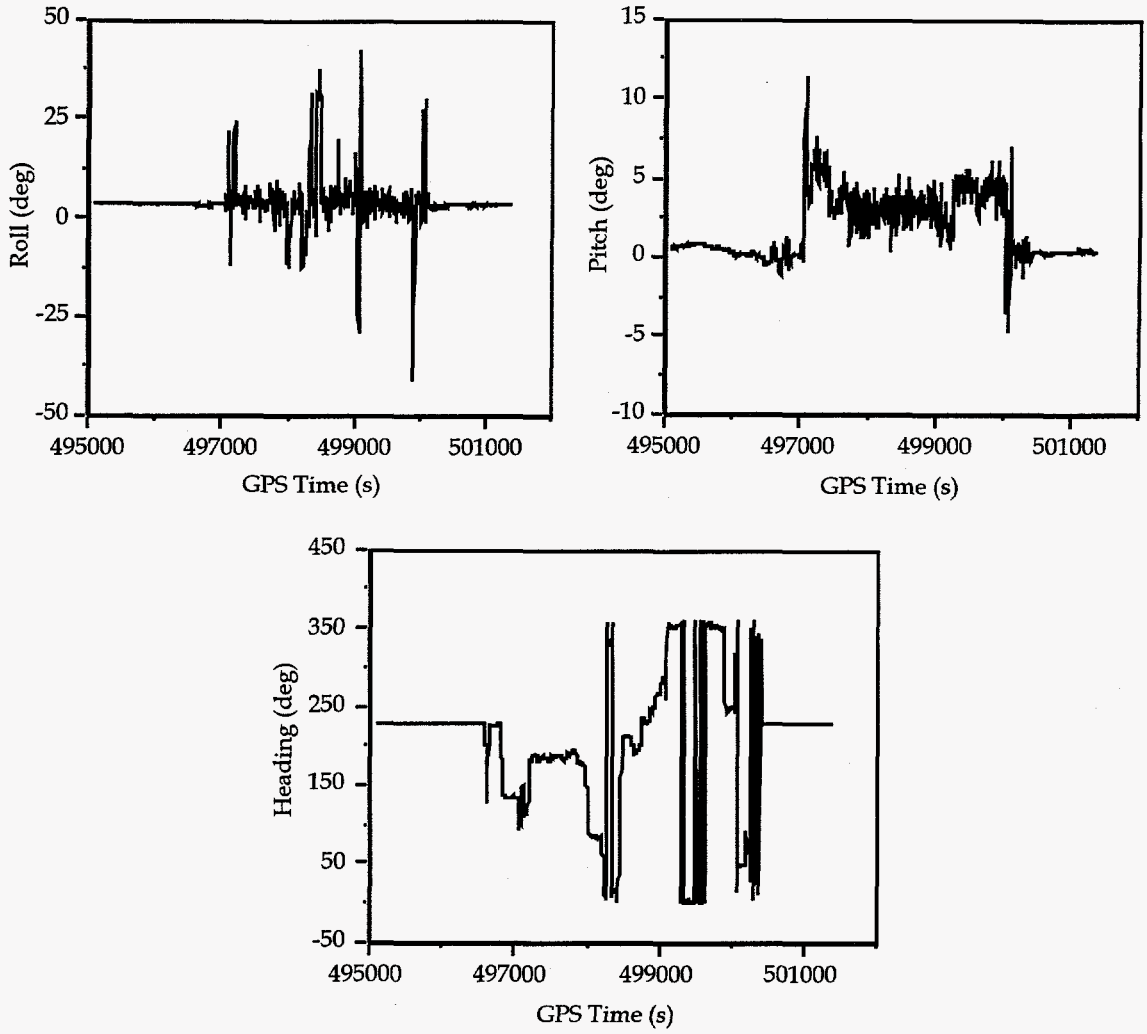

Figure 16. Aircraft Roll, Pitch and Heading on Day 4
Estimated from GPS

2.3.2 GPS Attitude Estimation Methodology

The GPS data was processed using The University of Calgary's MULTINAV™ software program which estimates roll, pitch and heading using carrier phase measurements from three or more antennas. The body frame, which is needed for definition of the aircraft attitude, was realized by three antennas, namely the aft, forward and port antennas. These are shown on Figure 17 below.

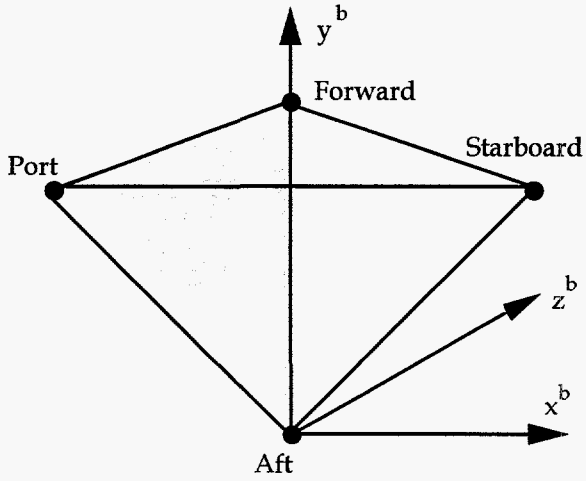

Figure 17. Body Frame Defined by GPS Antennas

The body frame can be measured directly or can be determined by GPS initialization, which is typically more convenient. In this case, the body frame was determined through a two hour static GPS survey when the aircraft was located on the tarmac prior to take-off. The resulting body frame coordinates are shown in Table 8. Distances between the GPS antenna pairs were estimated to about the 1 cm level and were used as constraints in the attitude determination algorithm to eliminate incorrect carrier phase integer ambiguities during the search phase.

Table 8. Antenna Body Frame Coordinates

Antenna	x (m)	y (m)	z (m)
1 (aft)	0.0000	0.0000	0.0000
2 (forward)	0.0000	6.9222	0.0000
3 (port)	-9.5141	4.8085	0.0000
4 (starboard)	9.1555	5.5115	0.9335

Attitude components, i.e. roll, pitch and heading, are estimated via a least squares approach using the interstation vectors between antennas as quasi-observables. Suppose $r_i^b = (x_i^b, y_i^b, z_i^b)^T$ are the body-frame coordinates of the i-th antenna which were previously estimated. The measurements are $r_i^n = (x_i^n, y_i^n, z_i^n)^T$, the local level coordinate

of the i-th antenna, which are determined from the differential GPS carrier phase solution. These coordinates satisfy the following equation

$$\begin{pmatrix} r_2^b \\ r_3^b \\ r_4^b \end{pmatrix}^T = R_n^b(\varphi,\theta,\psi) \begin{pmatrix} r_2^n \\ r_3^n \\ r_4^n \end{pmatrix}^T$$

where $R_n^b(j,q,y)$ is the transformation matrix between the body-frame coordinates and the local-level frame coordinates, and

$$R_n^b(j,q,y) = \begin{pmatrix} c(y)c(j)-s(y)s(q)s(j) & s(y)c(j)+c(y)s(q)s(j) & -c(q)s(j) \\ -s(y)c(q) & c(y)c(q) & s(q) \\ c(y)s(j)+s(y)s(q)c(j) & s(y)s(j)-c(y)s(q)c(j) & c(q)c(j) \end{pmatrix}$$

where c() is a cosine function and s() is a sine function. When there are three antennas on the platform, a unique solution is generated, whereas a fourth antenna provides redundancy. These equations can be solved using a least squares adjustment model by minimizing the cost function

$$J(\varphi,\theta,\psi) = \left\| (r^b - R(\varphi,\theta,\psi) r^n \right\|^2$$

The least squares method has many advantages over other methods such as a direction computation of attitude (Lu et al., 1993). It can easily accommodate more antennas and attitude is less effected by multipath from a single antenna since it is based on a least squares fit of all antenna positions.

Further details on the methodology used in the attitude determination algorithms are given in Lachapelle et al. (1994) and Lu (1994).

2.3.3 Wing Flexure Modeling

Due to wing flexure of the aircraft, the body-frame defined above is not a fixed rigid body frame. Since the frame is changing with the wing flexure, the derived attitude is relative to a different coordinate frame. In order to obtain attitude with respect to one fixed coordinate frame, the wing flexure has to be removed before attitude is computed. A wing flexure model was considered here. Wing flexure is constrained in the z- component in the body frame. That is

$$r_i^b = r_i^{b0} - B_f f$$

where

$$B_f = (0,0,1)^T$$

and f is a scalar amount which is estimated in the least square adjustment.

When considering all four antennas, the body frame coordinates and the local level coordinates should satisfy the following relation

$$\begin{pmatrix} r_2^b \\ r_3^b \\ r_4^b \end{pmatrix}^T = \begin{pmatrix} r_2^{b0} \\ r_3^{b0} \\ r_4^{b0} \end{pmatrix}^T - \begin{pmatrix} 0 & 0 & 0 \\ 0 & 0 & 0 \\ 1 & 0 & 1 \end{pmatrix} f \ .$$

The solution is obtained by minimizing the cost function

$$J(\varphi,\theta,\psi,f) = \left\| (r^{b0} - Bf) - R(\varphi,\theta,\psi) r^n \right\|^2 .$$

Refer to Cohen et al. (1993) for a similar approach to flexure modeling.

2.3.4 INS Attitude Reference

The INS attitude parameters were collected to provide a reference for the analysis of the non-dedicated GPS attitude system. Roll, pitch and heading which were output from the real-time navigation filter were used for this purpose. The accuracy of the roll and pitch reference values are at the level of 1 arcminute given the system installed on the aircraft, whereas the heading accuracy is accurate to 4-5 arcminutes. It should be noted that the heading error is generally a bias and is removed when comparison with the GPS heading is done by the development of a rotation matrix as discussed below.

2.3.5 GPS - INS Comparison Strategy

In order to compare the GPS and INS attitude parameters, errors in the alignment of one system with respect to the other must be taken into account. These misalignment errors are inevitable due to the difficulties in mounting the systems in the aircraft.

The rotation matrix that represents the mounting error is R_I^G which is the rotation required to transform the INS attitude parameters to the GPS body frame. It is computed as

$$R_I^G = R_I^n \, R_n^G$$

where R_I^n is the INS to local level transformation which can be formed using the INS output attitude parameters while R_n^G is the local level to GPS body frame transformation matrix which can be formed using attitude parameters computed from the GPS multi-antenna system. The matrix R_I^G is determined at each epoch of the flight data and then a mean transformation for the mission is determined. This transformation matrix was determined separately for each flight, however the agreement between the two days is at the 10 arcsec level which verifies the comparison strategy.

Results presented below are therefore the remaining differences between GPS and INS once the above rotation matrix has been applied. A similar implementation for GPS and INS comparisons can be found in Lachapelle et al. (1994).

2.3.6 Wing Flexure Results

In order to assess the impact of wing flexure modeling, comparisons are first made between the INS and GPS attitude parameters without the model being applied. Data from Day 4 was selected for this analysis.

Figure 18 gives the differences in roll, pitch and heading between the two systems for the entire mission. Results for the pitch and heading components are generally centered around zero, while the roll differences exhibit two clear discontinuities. Correlating these discontinuities with the vertical velocity profile in Figure 19, it shows that they occur when the aircraft takes off and lands and thus is most likely due to wing flexure. Due to the low correlation of wing flexure versus pitch and heading, no significant effects are present.

The GPS attitude data was then re-processed with the flexure model implemented. Estimated wing flexure from the model is shown in Figure 20 and demonstrates flexure at the level of 12 cm. The plot in this figure is highly correlated to the roll differences shown in Figure 18, which confirms that the discontinuities are in fact due to flexure.

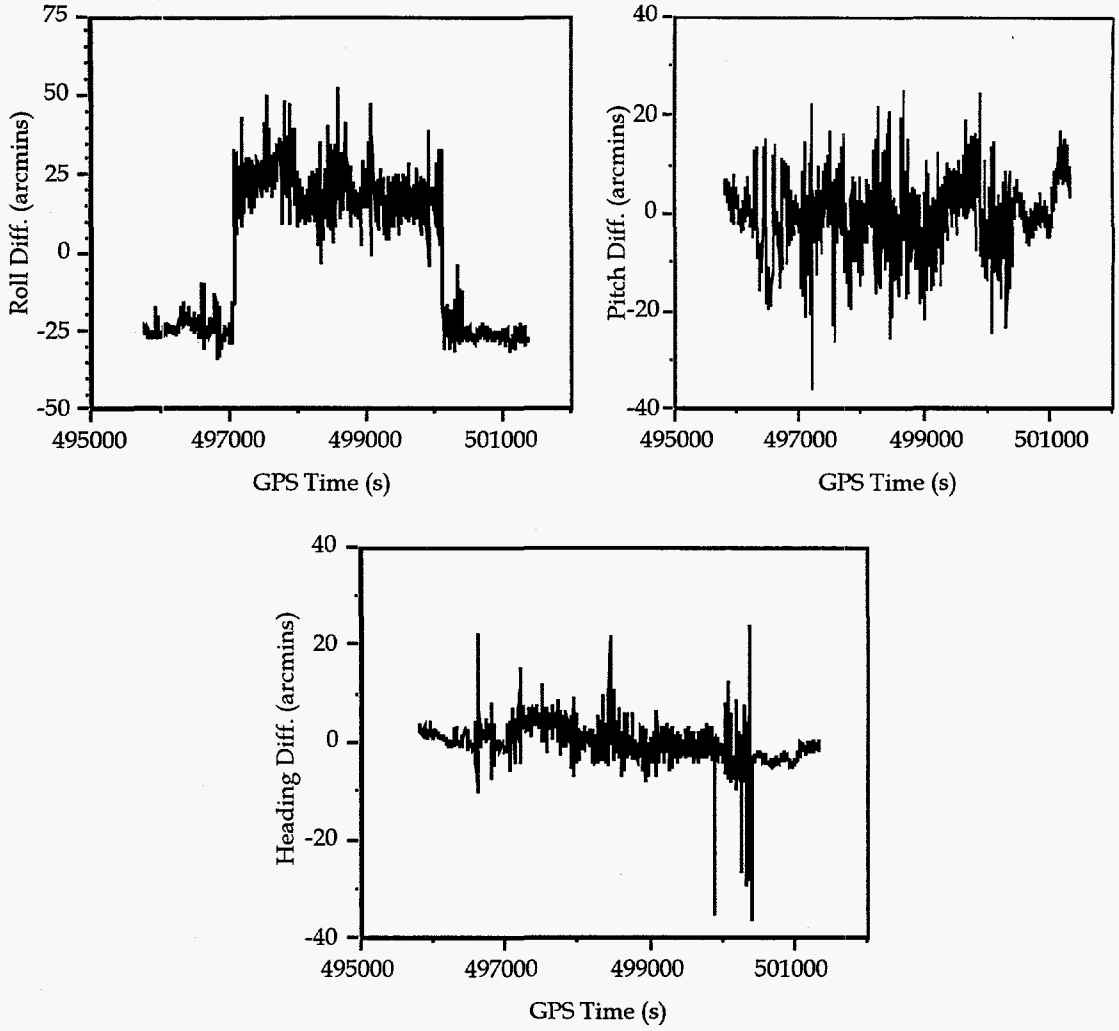

Figure 18. GPS-INS Attitude Differences on Day 4 without Wing Flexure Model

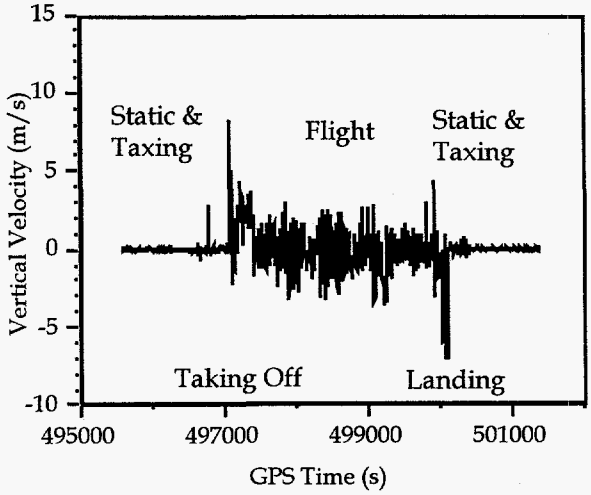

Figure 19. Vertical Aircraft Velocity on Day 4

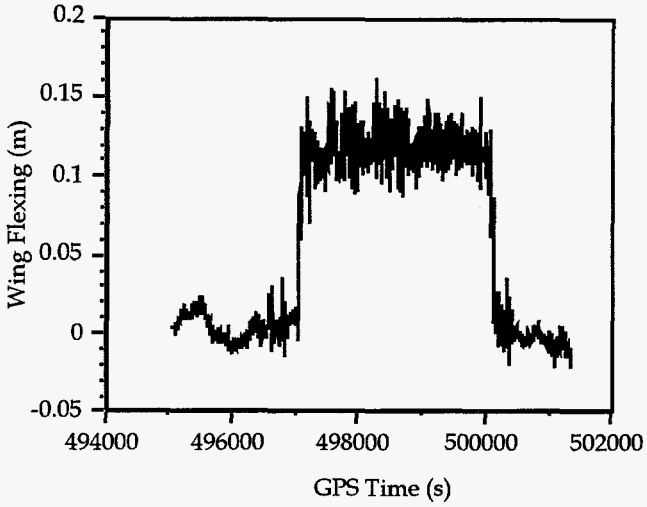

Figure 20. Estimated Wing Flexure on Day 4

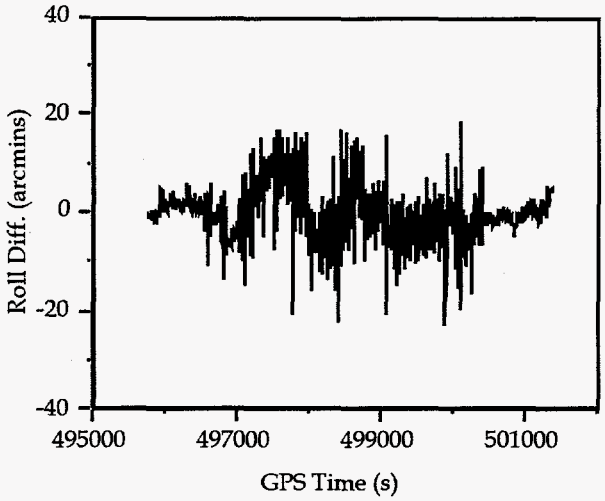

Figure 21. GPS-INS Roll Differences on Day 4 with Wing Flexure Model

A comparison of the re-processed roll component with wing flexure removed is plotted in Figure 21. The discontinuities are eliminated and the remaining errors are thus carrier phase noise and multipath. The effect of multipath has an amplitude of 10-12 arcminutes in terms of roll. These results, along with those obtained for the Day 3 test are discussed in further detail below.

2.3.7 GPS-INS Attitude Agreement

From Figure 21, the most significant remaining errors are the carrier phase noise as well as mulitpath. Additional errors are due to high frequency wing vibration and small time tagging errors between the GPS and INS systems.

Figure 22 shows the estimated wing flexure for the Day 3 test. At approximately 418700 s the aircraft takes off and the wings flex about 10 to 12 cm as in the Day 4 case.

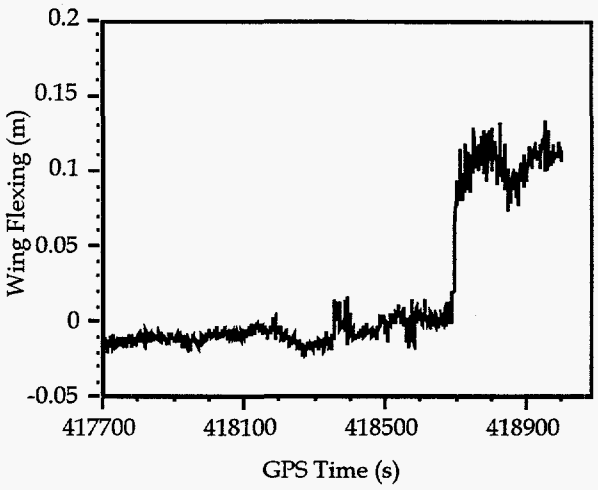

Figure 22. Estimated Wing Flexure on Day 3

Plotted in Figure 23 are the GPS versus INS differences with the wing flexure model applied. As in the Day 4 results, remaining errors are most likely due to noise and multipath. At time 418350 s there is a fluctuation in the agreement at the level of +/- 20 arcminutes which occurs when the aircraft makes a sharp turn on the ground before take-off. A similar phenomenon occurs in the Day 4 results at time 500400 s after the aircraft lands (see Heading plot in Figure 18). This also coincides with a sharp turn on the ground after landing.

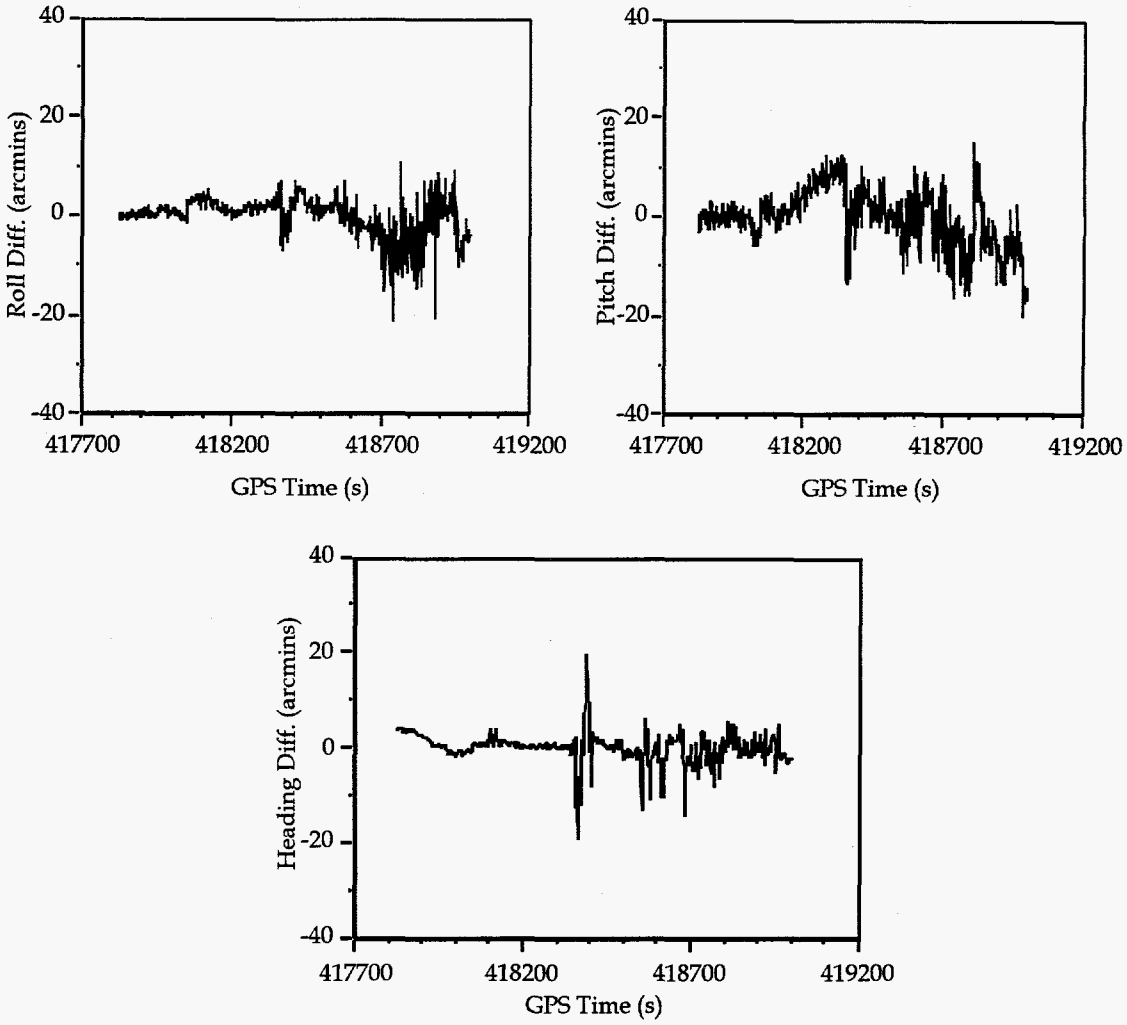

Figure 23. GPS-INS Differences on Day 3 with Wing Flexure Model

Table 9 summarizes the statistics of the GPS-INS differences. Agreement is at the level of 3.1 to 6.6 arcminutes for the three components which agrees well previous results using a non-dedicated GPS attitude determination system, e.g. Lu et al. (1993), as well as those obtained from fully dedicated systems, e.g. Schade et al. (1993). Results for the Day 4 test are slightly degraded with respect to those from Day 3 which is due to the shorter flight segment on Day 3 (i.e. more static data is included in the results).

Table 9. RMS of the Differences Between GPS and INS Attitude

Session	RMS (arcmins)		
	Roll	Pitch	Heading
Day 3	3.6	5.0	3.1
Day 4	5.0	6.6	3.9

2.3.8 GPS Attitude Determination Test Conclusions

Several flight tests were conducted using a non-dedicated GPS attitude determination system consisting of four NovAtel GPSCard™ receivers installed in a Twin Otter aircraft. An INS was also mounted in the aircraft to provide an attitude reference at the level of 1 arcminute. Roll and pitch angles ranged from -5 to 12 degrees and -40 to +45 degrees, respectively during the tests.

In order to properly compare the GPS and INS attitude parameters, a wing flexure model was introduced into the GPS model. Flexure was then estimated at each measurement epoch. The most significant effects were found at take-off and during landing when the flexure reached approximately 12 centimeters.

Once flexure was taken into account the agreement between GPS and INS attitude was at the level of 3-7 arcminutes. Given that the distances between the antennas ranged from 7 to 10 m, this level of compatibility agrees with previous flight tests using dedicated systems, as well marine tests using a similar non-dedicated approach discussed above. The advantages of the non-dedicated approach is twofold; firstly to provide flexibility in the installation and usage of the GPS receivers, and secondly to provide a cost-effective system which can use emerging low-cost GPS receivers which output the carrier phase observable.

The attitude accuracy achieved by the multiple antenna GPS system is probably not at the level where it would significantly enhance the INS attitude error estimation capability of an integrated GPS/INS system with an INS the quality of the RLGA (0.01 degrees/per hour), but it might prove useful in aiding lower quality IMUs containing gyros with higher drift rates. A GPS-based attitude determination capability would also enhance INS in-flight alignment performance.

3. SAR TARGET LOCATION APPLICATION

3.1 Introduction to SAR Target Location

Applications of this precise GPS/INS integration include synthetic aperture radar (SAR) target location and interferometric SAR (IFSAR) image formation and three dimensional target location.

This section addresses the question of the real time geographic target location accuracy achievable by an surveillance SAR in a single pass by the target. This technique assumes a tightly integrated GPS/INS/IFSAR system. The interferometric SAR (IFSAR) provides not only the adverse weather imaging capability of radar, but also an accurate capability to measure both relative and absolute heights of the target and terrain in a single pass by the target, see Bickel and Hensley (1996). The GPS/INS unit provides the position and velocity data necessary to tie the two dimensional azimuth/range SAR image to a geographic frame and, for the IFSAR, also provides the antenna attitude measurements required to calculate height information relative to the aircraft. Improvement in the accuracy of the integrated GPS/INS system's position, velocity, and attitude solution reduces the IFSAR's target location error. An example IFSAR image is shown in Figure 24 below, with a corresponding optical photo of the same area.

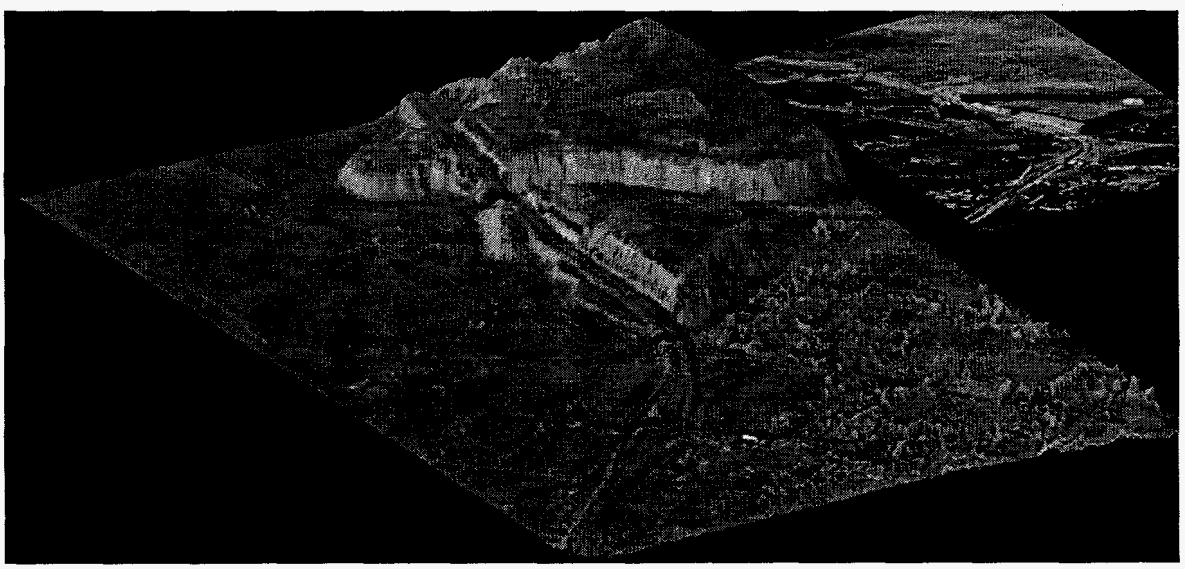

Figure 24. Three Dimensional IFSAR Terrain Map

3.2 Target Location Error

The target geographic location error can be divided into three major error components:

a) The motion measurement and SAR/IFSAR processing errors which produce a relative three dimensional position error between the airborne platform and the ground target.

b) The random component of the air vehicle's position error, and

c) The long time constant or bias in the air vehicle's position error caused by errors in the GPS constellation broadcast ephemeris, clock, and atmospheric propagation delays.

The incorporation of GPS carrier phase measurements into the SAR/IFSAR motion measurement system can significantly reduce the random component of the vehicle's position error. The noise of the carrier phase measurement is on the order of several millimeters as compared to 1 to 2 meters for the code-derived range measurement. Also, multipath effects, in which the received GPS signal has reflected off of one or more structures before reaching the receiving antenna, that contribute to position errors are greatly reduced by utilizing GPS carrier phase measurements.

The motion measurement and SAR processing errors may be further broken into cross line-of-sight, along line-of-sight, and height errors.

3.2.1 Cross Line-of-Sight Geographic Location Error:

The primary contributor to cross line-of-sight SAR error is the line-of-sight velocity error of the motion measurement system which is used to resolve Doppler shift into azimuth location during the SAR image formation process. This error is given by:

$$\frac{R * Vlos_{err}}{V_x * \sin\alpha}$$

where

R = line-of-sight range (m)
$Vlos_{err}$ = line-of-sight velocity error (m/s)
V_x = along track velocity (m/s)
α = squint angle defined to be the aircraft's ground track angle - angle from aircraft to target.

Therefore, the contribution of velocity error in the motion measurement system to cross line-of-sight position error increases linearly with range and diminishes with higher aircraft velocities. For the case of the current SAR system in the Twin Otter, using our existing real time integrated GPS/INS system which does not use carrier phase measurements, typical values are R = 5,000 m, $Vlos_{err}$ = 0.05 m/sec, V_x=50 m/sec and a

squint angle of 90 degrees, the resulting cross line-of-sight location error is approximately 5 meters.

Any reduction in the average line-of-sight velocity error over the time interval necessary to form the SAR image (from a few seconds to a few minutes) will reduce this error component. Based on the agreement between the GPS and GPS/INS test results, the $Vlos_{err}$ could be reduced to 0.01 m/sec with the addition of carrier phase aiding, reducing the cross line-of-sight position error to 1 meter.

Other error sources that affect cross line-of-sight geographic location error include pixel designation error in the two dimensional SAR slant plane, timing errors between the motion measurement system and the SAR image formation process, and GPS position errors.

3.2.2 Along Line-of-Sight Geographic Location Errors

The primary contributors to along line-of-sight errors are any uncalibrated SAR range biases, pixel designation error in the SAR image, motion measurement to SAR image formation timing errors if the imaging geometry includes squint, GPS position errors, and the projection of random and bias IFSAR height errors onto the ground plane. The height errors will be addressed in detail in the following section.

3.2.3 Height Error Sources

The IFSAR height error is composed of a random term and a bias term. The noise term is given by:

$$\frac{\lambda \, R \cos \Phi}{4\pi \, B \, \sqrt{N * SNR}}$$

where:

λ - is the SAR wavelength
R - is the range from the aircraft to the center of the scene
Φ - is the depression angle to the center of the scene
B - is the IFSAR phase center separation distance
N - is the number of range and azimuth pixels to combine to form a height estimate
SNR - is the signal to noise ratio.

The height error bias term is driven primarily by the error in measuring the roll angle of

the IFSAR antenna and by phase errors between the two antennas. It is given by:

$$R \sin(e_{roll})\cos(\Phi) + \frac{\lambda R \quad e_{phase} \cos(\Phi)}{4\pi B}$$

where:

e_{roll} - is the IFSAR antenna pointing error
e_{phase} - is the phase error between the two IFSAR antennas.

The inclusion of GPS carrier phase measurements into the integrated GPS/INS solution not only reduces the position and velocity errors, but also, due to the much lower random noise value of carrier phase measurements as compared to code derived range, range rate, position, and velocity measurements, the Kalman filter can better estimate the INS' attitude errors and thus reduce the IFSAR antenna pointing error component.

4. REFERENCES

Bickel, D.L. and Hensley, W.H. (1996), Design, Theory, and Applications of Interferometric Synthetic Aperture Radar For Topographic Mapping, Sandia Report, SAND96-1092.

Cannon, M.E. (1990), High-Accuracy GPS Semikinematic Positioning: Modeling and Results, Navigation, Journal of the Institute of Navigation, Vol. 37, No. 1, pp. 53-64.

Cannon, M.E. (1991), Airborne GPS/INS with an Application to Aerotriangulation, Report No. 20040, Department of Surveying Engineering, The University of Calgary.

Cannon, M.E., and G. Lachapelle (1992), Analysis of a High Performance C/A Code GPS Receiver in Kinematic Mode, Navigation, Vol. 39, No.3, pp 285-299.

Cannon, M.E., Sun, H. Owen, T.E. and Meindl, M.A. (1994), Assessment of a Non-Dedicated GPS Receiver System for Precise Airborne Attitude Determination, Proceedings of ION GPS-94, Salt Lake City, September 20-23, pp. 645-654.

Cohen, C.E. and B.W. Parkinson (1992), Aircraft Applications of GPS-Based Attitude Determination, Proceedings of ION GPS-92, Albuquerque, September 16-18, pp. 775-782.

Cohen, C.E., B.D. McNally and B.W. Parkinson (1993), Flight Tests of Attitude Determination Using GPS Compared Against an Inertial Navigation Unit, Navigation, Journal of the Institute of Navigation, Vol. 41, No. 1, pp. 83-97.

Fellerhoff, J.R. and S.M. Kohler (1992), Development of a GPS-Aided Motion Measurement, Pointing and Stabilization System for a Synthetic Aperture Radar, Proceedings of the 48th ION Annual Meeting, Washington, D.C., June 29-July 1, pp. 291-296.

Ferguson, K., J. Kosmalska, M. Kuhl, J.M. Eichner, K. Kepski and R. Abtahi (1991), Three Dimensional Attitude Determination with the Ashtech 3DF 24 Channel GPS Measurement System, Proceedings of the ION NTM, Phoenix, January 22-24, pp. 35-41.

Johnson, L. (1996), Tonopah Test Range Outpost of Sandia National Laboratories, Sandia Report, SAND96-0375.

Lachapelle, G., M.E. Cannon , and G. Lu (1993), A comparison of P Code and High Performance C/A Code GPS Receivers for On The Fly Ambiguity Resolution, Bulletin Géodésique, Vol. 18, No. 3, pp. 185-192.

Lachapelle, G., G. Lu, and B. Loncarevic (1994), Precise Shipborne Attitude Determination Using Wide Antenna Spacing, Proceedings of the International Symposium on Kinematic Systems in Geodesy, Geomatics and Navigation - KIS94, Banff, August 30-September 2.

Lu, G., M.E. Cannon, G. Lachapelle, and P. Kielland (1993) Attitude Determination in a Survey Launch Using Multi-Antenna GPS Technologies, Proceedings of the ION National Technical Meeting, San Francisco, January 20-22, pp. 251-260.

McMillan, J.C., D.A.G. Arden, G. Lachapelle, and G. Lu (1994) Dynamic GPS Attitude Performance Using INS/GPS Reference, Presented at the ION GPS94, Salt Lake City, September 21-23.

Owen, T.E. and R. Wardlaw (1992), Evaluating the Velocity Accuracy of an Integrated GPS/INS System: Flight Test Results, Proceedings of the ION National Technical Meeting, San Diego, January 27-29, pp.13-22.

Schade, H., M.E. Cannon and G. Lachapelle (1993), An Accuracy Analysis of Airborne Kinematic Attitude Determination with the NAVSTAR/Global Positioning System, SPN Journal, Vol. 3, No. 2, pp. 90-95.

Schwarz, K.P., A. El-Mowafy and M. Wei (1992), Testing a GPS Attitude System in Kinematic Mode, Proceedings of ION GPS92, Albuquerque, September 16-18, pp. 801-809.

Sun, H., Cannon, M.E., Owen, T.E., and Meindl, M.A. (1994), An Investigation of Airborne GPS/INS for High Accuracy Position and Velocity Determination, Proceedings of the ION National Technical Meeting, San Diego, January 24-26, pp. 801-809.

Sun, H. (1994), Integration of INS with Multiple GPS Antennas for Airborne Applications, Proceedings of ION GPS94, Salt Lake City, September 21-23, pp. 1401-1409.

Tiemeyer, B., M.E. Cannon, G. Lu and G. Schänzer (1994), Satellite Navigation for High Precision Aircraft Navigation with Emphasis on Atmospheric Effects, To be presented at the IEEE PLANS'94, Las Vegas, April 12-15.

Van Graas, F. and M. Braasch (1991), GPS Interferometric Attitude and Heading Determination: Initial Flight Test Results, Navigation, Journal of The Institute of Navigation, Vol. 38, No. 4, pp. 297-316.

Distribution:

1	0537	D. L. Bickel, 2344
1	0537	W.H. Hensley, 2344
1	0860	E. E. Jones, 2522
1	0860	F. J. Perdreauville, 2522
1	0843	J. D. Bradley, 2525
1	0843	M. C. Dowdican, 2525
10	0843	J. R. Fellerhoff, 2525
1	0843	T. J. Kim, 2525
10	0843	T. E. Owen, 2525
1	0843	M. L. Pedroncelli, 2525
10	1174	M. A. Meindl, 2526
1	1174	A. C. Watts, 2526
3	0188	Charles E. Meyers, 4523
1	0570	B. F. Johnson, 5900
1	0572	C. V. Jakowatz, 5912
1	9018	Central Technical Files, 8940-2
5	0899	Technical Library, 4414
2	0619	Review & Approval Desk, 12690 For DOE/OSTI